

1 Excessive inflammatory and metabolic responses to acute SARS-CoV-2 infection
2 are associated with a distinct gut microbiota composition

3

4 Werner C. Albrich^{1*}, Tarini Shankar Ghosh^{2,3*}, Sinead Ahearn-Ford³, Flora
5 Mikaeloff⁴, Nonhlanhla Lunjani^{3,5}, Brian Forde^{2,3}, Noémie Suh⁶, Gian-Reto Kleger⁷,
6 Urs Pietsch⁸, Manuel Frischknecht¹, Christian Garzoni^{9,10}, Rossella Forlenza¹⁰, Mary
7 Horgan^{11,12}, Corinna Sadlier^{11,12}, Tommaso Rochat Negro⁶, Jérôme Pugin⁶, Hannah
8 Wozniak⁶, Andreas Cerny¹⁰, Ujjwal Neogi⁴, Paul W. O'Toole^{2,3}, Liam O'Mahony^{2,3,11}

9

10 *Both authors share first authorship

11 ¹Division of Infectious Diseases & Hospital Epidemiology, Cantonal Hospital St.
12 Gallen, Rorschacherstrasse 95, 9007 St. Gallen, Switzerland

13 ²School of Microbiology, University College Cork, National University of Ireland,
14 Cork, Ireland

15 ³APC Microbiome Ireland, University College Cork, National University of Ireland,
16 Cork, Ireland

17 ⁴The Systems Virology Lab, Division of Clinical Microbiology, Department of
18 Laboratory Medicine, Karolinska Institute, ANA Futura, Campus Flemingsberg,
19 Stockholm, Sweden.

20 ⁵Department of Dermatology, University of Cape Town, Cape Town, South Africa.

21 ⁶Division of Intensive Care, Geneva University Hospitals and the University of
22 Geneva Faculty of Medicine, 1211 Geneva, Switzerland

23 ⁷Division of Intensive Care, Cantonal Hospital St. Gallen, Rorschacherstrasse 95,
24 9007 St. Gallen, Switzerland

25 ⁸Department of Anesthesia, Intensive Care, Emergency and Pain Medicine,
26 Cantonal Hospital St. Gallen, Rorschacherstrasse 95, 9007 St. Gallen, Switzerland.

27 ⁹Clinic of Internal Medicine and Infectious Diseases, Clinica Luganese Moncucco,
28 Lugano, Switzerland; Department of Infectious Diseases, Bern University Hospital,
29 University of Bern, Bern, Switzerland.

30 ¹⁰Fondazione Epatocentro Ticino, Via Soldino 5, 6900 Lugano, Switzerland.

31 ¹¹Department of Medicine, University College Cork, National University of Ireland,
32 Cork, Ireland.

33 ¹²Department of Infectious Diseases, Cork University Hospital, Cork, Ireland

34

35 Corresponding Authors:

36 Prof. Liam O'Mahony, Dept. of Medicine and School of Microbiology, APC

37 Microbiome Ireland, University College Cork, Cork, Ireland.

38 liam.omahony@ucc.ie

39 Prof. Werner Albrich, Division of Infectious Diseases & Hospital Epidemiology,

40 Cantonal Hospital St. Gallen, Rorschacherstrasse 95, 9007 St. Gallen, Switzerland.

41 werner.albrich@kssg.ch

42

43

44 **Abstract**

45 Protection against severe acute respiratory syndrome coronavirus 2 (SARS-
46 CoV-2) infection and associated clinical sequelae requires well-coordinated
47 metabolic and immune responses that limit viral spread and promote recovery of
48 damaged systems. In order to understand potential mechanisms and interactions
49 that influence coronavirus disease 2019 (COVID-19) outcomes, we performed a
50 multi-omics analysis on hospitalised COVID-19 patients and compared those with
51 the most severe outcome (i.e. death) to those with severe non-fatal disease, or
52 mild/moderate disease, that recovered. A distinct subset of 8 cytokines and 140
53 metabolites in sera identified those with a fatal outcome to infection. In addition,
54 elevated levels of multiple pathobionts and lower levels of protective or anti-
55 inflammatory microbes were observed in the faecal microbiome of those with the
56 poorest clinical outcomes. Weighted gene correlation network analysis (WGCNA)
57 identified modules that associated severity-associated cytokines with tryptophan
58 metabolism, coagulation-linked fibrinopeptides, and bile acids with multiple
59 pathobionts. In contrast, less severe clinical outcomes associated with clusters of
60 anti-inflammatory microbes such as *Bifidobacterium* or *Ruminococcus*, short chain
61 fatty acids (SCFAs) and IL-17A. Our study uncovered distinct mechanistic modules
62 that link host and microbiome processes with fatal outcomes to SARS-CoV-2
63 infection. These features may be useful to identify at risk individuals, but also
64 highlight a role for the microbiome in modifying hyperinflammatory responses to
65 SARS-CoV-2 and other infectious agents.

66 **Introduction**

67 Infection with SARS-CoV-2 leads to a wide variety of potential outcomes from
68 asymptomatic responses to acute respiratory distress and death^{1,2}. While certain
69 demographic factors such as age, male gender and comorbidities that include
70 obesity, cardiometabolic diseases and diabetes are associated with an increased
71 risk for more severe disease, the molecular mechanisms that underpin disease
72 pathophysiology remain poorly understood. Indeed, we still do not know if severe
73 outcomes are due to direct effects of viral replication within target cells, to a
74 dysregulated host immune response to the virus, to pre-existing deficits in
75 mechanisms of host resilience to infection, or to a combination of these factors^{3,4,5}.

76 Initially SARS-CoV-2 infects angiotensin-converting enzyme 2 (ACE-2)
77 expressing epithelial cells of the upper respiratory tract. If the infection remains
78 limited to the upper respiratory tract then this is usually associated with a mild
79 disease course and rapid recovery. If the virus is not eliminated and infection
80 persists then other types of ACE-2 expressing cells can become infected⁶. In
81 addition, viral-induced metabolic reprogramming and exaggerated immune
82 responses generate a wide range of inflammatory mediators that disrupt organ
83 homeostasis, impact host metabolism, drive a hypercoagulation state, impair
84 epithelial barrier function and destroy host cells and tissues^{7,8,9,10,11}. However, even
85 among those who develop this cytokine storm, many can still make a full recovery,
86 suggesting that additional factors may modulate host susceptibility to the most
87 severe outcomes associated with COVID-19. One of these resilience factors might
88 include the microbiome^{12,13,14,15}.

89 Human mucosal surfaces and body cavities harbour diverse communities of
90 commensal microbes that play essential roles in regulation of host metabolic

91 responses, epithelial barrier function, immune education and immune
92 regulation^{16,17,18,19,20}. These effects are partially induced by activation of host pattern
93 recognition receptors to microbial-derived danger signals, but increasingly the role
94 for bacterial metabolites in shaping host immune function is being recognised^{21,22,23}.
95 Immunoregulatory bacterial metabolites can trigger host G protein-coupled receptors
96 (GPCRs), aryl hydrocarbon receptors (AhRs), nuclear hormone receptors such as
97 the farnesoid X receptor, or can directly modulate gene expression through
98 epigenetic mechanisms. Importantly, many immunoregulatory bacterial metabolites
99 are derived from dietary substrates (e.g. fiber), linking diet and lifestyle to protection
100 from infection via microbial mechanisms.

101 In this study, our primary aim was to identify the immune-metabolic-microbial
102 interactions and biomarkers that predict the most severe outcomes to SARS-CoV-2
103 infection in a well characterised cohort of patients hospitalised with COVID-19. In
104 addition, we wished to identify clusters of patient metadata features that might
105 provide novel mechanistic insights into the disease pathophysiology. Lastly, we
106 wished to extend our understanding of the molecular processes within the holobiont
107 that mediate resilience to severe biological challenges, such as viral infection.

108 **Results**

109 *Systemic levels of immune mediators correlate with disease severity*

110 While changes in circulating cytokine levels due to SARS-CoV-2 infection are
111 already well described, the immune mediators that distinguish survivors from non-
112 survivors in severely ill patients have not been clearly identified. To better
113 understand the immune processes that might distinguish these patients, we
114 measured the levels of 54 immune mediators in the earliest serum sample obtained
115 following study enrolment after admission to the intensive care unit (ICU; severe
116 COVID-19) or the hospital ward (mild to moderate COVID-19) from 172 hospitalised
117 patients with PCR-confirmed SARS-CoV-2 causing COVID-19. Patient demographic
118 details are shown in Table 1. Those with mild/moderate COVID-19 (n=42) were
119 younger, more likely to be female, less frequently obese, required fewer medications
120 and had fewer comorbidities compared to those with severe COVID-19 (n=130).
121 However, there were no differences in demographics, medication use or
122 comorbidities in those severely ill patients that survived infection (n=89), compared
123 to those COVID-19 patients with a fatal outcome (n=41). In contrast, principal
124 component analysis of serum immune mediators demonstrated a clear separation
125 between patients with different COVID-19 disease outcomes (Fig. 1a). Compared to
126 healthy volunteers (n=29), levels of 36 circulating immune mediators were
127 significantly differed (30 higher and 6 lower) in those hospitalised with COVID-19
128 (Fig. 1b and Supplementary Fig. 1). Of these mediators, levels of 28 were
129 significantly different between patients with mild/moderate COVID-19 compared to
130 patients with severe disease (Fig. 1b). Within the severely ill group, the levels of 8
131 circulating immune mediators (soluble intercellular adhesion molecule-1 (sICAM-1),
132 monocyte chemoattractant protein-1 (MCP-1), interleukin (IL)-8, macrophage-derived

133 chemokine (MDC), interferon gamma-induced protein-10 (IP-10), IL-15, IL-1 receptor
134 antagonist (RA) and thymic stromal lymphopoietin (TSLP)) were significantly
135 different between those that survived and those that died (Fig. 1b and Fig. 1c).

136

137 *Systemic metabolic responses associated with disease severity*

138 In addition to measuring serum cytokines, we quantified and compared
139 metabolite levels in the first serum sample obtained following study recruitment after
140 admission to the ICU or hospital ward for COVID-19 patients with mild/moderate
141 disease (n=25), COVID-19 patients with severe disease that survived (n=75) or
142 COVID-19 patients with severe disease that succumbed to death (n=39). Distinct
143 differences in circulating metabolites were evident between each of the groups (Fig.
144 2a and Fig. 2b). Metabolic processes were dramatically different in patients during
145 acute SARS-CoV-2 infection, whereby levels of 377 metabolites were significantly
146 different (adjusted $p < 0.05$) between healthy volunteers (n=20) and those with
147 mild/moderate COVID-19 (Fig. 2b). These differences were further exaggerated in
148 COVID-19 patients with severe disease (583 metabolites, adjusted $p < 0.05$), in
149 particular those with a fatal outcome (659 metabolites, adjusted $p < 0.05$), when
150 compared to healthy volunteers. Within the severely ill patients, 140 metabolites
151 distinguished those that survived versus those that died. The metabolites that
152 contribute most to the differences between the groups included those involved in
153 tryptophan metabolism, polyamine metabolism, histidine metabolism, lipid
154 metabolism, bile acid metabolism and antioxidant responses such as the
155 plasmalogens (Fig. 2c and Supplementary Fig. 2). Random forest analysis
156 suggested a good discriminatory power for distinguishing COVID-19 disease severity

157 or fatality based solely on a selection of circulating metabolites (Fig. 2c and
158 Supplementary Fig. 3), underlining the robustness of these differences.

159 Given the substantial and significant differences in metabolite levels, we
160 examined in more detail the most significantly impacted pathways that associated
161 with COVID-19 severity (Fig. 3a). Interestingly, levels of sulphonated bile acids were
162 particularly disrupted with disease severity. Host tryptophan metabolism was
163 associated with a heavy depletion of tryptophan, with enhanced generation of
164 kynurenate, kynurenine and quinolinate, at the expense of serotonin synthesis in
165 COVID-19 patients (Fig. 3a and Supplementary Fig. 4a). In contrast, microbial
166 tryptophan metabolites were present at lower levels in the serum of those with the
167 worst outcome (Fig. 3a and Supplementary Fig. 4b). Changes in circulating microbial
168 metabolites may be due in part to an impaired gut barrier (as indicated by increased
169 serum SCFA levels and lower citrulline levels, Supplementary Fig. 4c and 4d), or
170 may reflect changes in the composition or metabolism of the gut microbiome.
171 Overall, metabolites associated with microbial metabolism (as described by Bar et
172 al²⁴) were significantly altered in those with severe disease and those with a fatal
173 outcome (Supplementary Fig. 4e).

174 Next, we performed a weighted co-expression network analysis restricted to
175 the COVID-19 patients, to identify communities of co-abundant metabolites. Positive
176 correlations between metabolites (Spearman, adjusted $p < 0.0005$) were used to build
177 the network. The analysis identified six communities (c1-c6) of highly intercorrelated
178 metabolites based on the Leiden algorithm [2 iterations, ModularityVertexPartition,
179 weighted network (Fig. 3b)]. Primary and secondary bile acid metabolism are
180 contained in c3, SCFA in c5, while tryptophan and histidine metabolism are in c1, c2
181 and c5 (Fig. 3c). The central community (c1) with the most interconnected

182 metabolites, central metabolites, and greatest influence on the global dynamics of
183 the network includes mannose (Fig. 3d), which is a known inflammatory biomarker
184 and reported to be associated with COVID-19 severity²⁵. Furthermore, the
185 metabolites that are significantly different between COVID-19 severe patients with or
186 without a fatal outcome are primarily found within community c1 (Fig. 3e).

187

188 *Differences in the gut microbiome associate with disease severity and death*

189 To investigate the possible involvement of the gut microbiome in these
190 immune and metabolic changes, we profiled the microbiome by sequencing 16S
191 rRNA gene amplicons from the first faecal samples collected following study
192 recruitment after admission to the ICU or hospital ward for COVID-19. From the 99
193 hospitalised COVID-19 patients with available stool samples for 16S amplicon
194 sequencing, 32 had mild/moderate disease, 45 had severe disease and survived,
195 while the remaining 22 patients had severe disease with a fatal outcome. Global
196 measures of microbiome alpha diversity were not different between clinical groups,
197 with no significant difference detected in Shannon indices as well as in the number of
198 detected taxa at the level of Operational Taxonomic Units (OTUs), species or genus
199 levels between the three disease outcome groups (Supplementary Fig. 5). However,
200 Envfit-based analysis of the Principal Coordinates revealed a significant difference in
201 gut microbiome composition (beta diversity) between the three COVID-19 disease
202 severity groups, irrespective of the distance measures used (Fig. 4a and
203 Supplementary Fig. 6). We next investigated these differences in microbiome profiles
204 in an unsupervised manner, i.e. without utilizing the disease outcome information.
205 Using an iterative enterotyping-based approach applied on the Principal coordinates
206 (See Methods), the microbiomes could be optimally clustered into two configurations

207 (MicrobiomeGroup1 and MicrobiomeGroup2), resolved clearly along the first
208 Principal Coordinate (Fig. 4b and 4c). Notably, there were significant differences in
209 the proportions of the two distinct microbiome configurations in the clinical outcome
210 groups (Chi-square test estimate=11.23, p-value = 0.0036, Fig. 4d).
211 MicrobiomeGroup1 was over-represented in severe COVID-19 patients with a fatal
212 outcome, while Microbiome Group2 was associated with those with mild/moderate
213 symptoms. Strikingly, within the severe outcome group, individuals who were
214 classified into the high-risk MicrobiomeGroup1 had significantly higher levels of
215 cytokines associated with both fatality and severity (P = 0.02; Mann-Whitney Test),
216 with higher (albeit not statistically significant) levels of cytokines associated only with
217 disease severity (P = 0.12, Mann-Whitney Test) (Supplementary Fig. 7).

218 We next investigated the genus-level composition differences across the two
219 microbiome configurations by performing ordinary-least square (OLS)-based
220 regression analysis to measure the association between abundance of microbial
221 genera and the PCo1 axis values after adjusting for confounders. A total of 9 genera
222 showed significant associations with PCo1 with FDR ≤ 0.15 (Benjamini-Hochberg
223 corrected), even after confounder adjustment. While two genus-level groups
224 (*Enterococcus* and an unclassified member of the *Enterococcaceae*) were
225 associated negatively with PCo1 (high relative abundance in the high risk
226 MicrobiomeGroup1), the other 7 (comprising *Christensenellaceae*-R7, *Dorea*,
227 *Fusicatenibacter* and multiple *Ruminococcus* species) showed the opposite trend
228 (Fig. 4e). Relaxing the thresholds identified 19 more genera that showed nominally
229 significant association with PCo1 (P ≤ 0.05). The high risk MicrobiomeGroup1 was
230 characterized by higher levels of multiple pathobionts (as operationally defined in our
231 previous work^{26,27}) including *Enterococcus*, *Eggerthella*, *Lachnoclostridium*,

232 *Erysipelatoclostridium*, *Streptococcus*, *Flavonifractor* and lower levels of multiple
233 taxa known to be associated with anti-inflammatory or protective immune responses
234 (including *Faecalibacterium*, *Agathobacter*, *Dorea*, *Coprococcus*, *Lachnospiraceae*,
235 *Christensenellaceae*) (Fig. 4e). Many of the observed differences in the microbiome
236 were significantly associated with changes in levels of circulating immune mediators
237 (Supplementary Fig. 8).

238

239 *Immune-metabolite-microbiome modules correlate with COVID-19 disease outcomes*

240 Correlation network analysis is a powerful tool for revealing associations of
241 diverse features within patient datasets. Feature-association networks were
242 computed using the Weighted gene correlation network analysis (WGCNA) approach
243 (see Methods) performed on 1,469 features (54 cytokines, 1,146 metabolites and
244 269 microbial genera) using signed Spearman correlations with a soft-power
245 threshold of 7 (Supplementary Figure 9a) from the 70 hospitalised COVID-19
246 patients with complete data for all three data layers. A total of 14 modules (annotated
247 as different colors) were identified, 5 of which had a significant association with
248 disease outcome (Benjamini-Hochberg $FDR \leq 0.05$) and 2 modules showed nominal
249 associations ($P \leq 0.05$ and $FDR \leq 0.1$) (Supplementary Fig. 9b-c). The module
250 (annotated as 'turquoise') that showed significant positive association with disease
251 severity and death contained most of the severity associated cytokines (as identified
252 in Fig. 1), metabolites (Supplementary Fig. 3) and microbial genera identified above
253 (Fig. 4e), combined with kynurenine associated metabolism products and
254 coagulation linked fibrinopeptides (Fig. 5a). Two modules (annotated as 'brown' and
255 'tan') were nominally positively associated with a poor outcome. Of these, the brown
256 module contained a triad of pathobionts linked to urobilinogen (Supplementary Fig.

257 10a), while the tan module was enriched for sulfonated bile acids (Supplementary
258 Fig. 10b). In contrast, 4 modules, annotated as 'red', 'blue', 'black' and 'yellow', were
259 significantly negatively associated with COVID-19 severity and death. The first
260 module (red) contained the anti-inflammatory *Ruminococcus_2* clade, linked with
261 tryptophan, alanine and the SCFAs butyrate/isobutyrate and valerate (Fig. 5b;
262 Supplementary Fig. 11). The second module (blue) that negatively associated with
263 disease severity contains a cluster of beneficial microbial taxa (including
264 *Bifidobacterium*), bilirubin degradation products, TARC and IL-17A (Supplementary
265 Fig. 12). The third module (black) exclusively contains metabolites, in particular fatty
266 acid derivatives (Supplementary Fig. 13), while the final significant module (yellow)
267 contains *Roseburia*, *Fusicatenibacter*, *Romboutsia* linked with sphingomyelin and
268 carnitine-derived products (Supplementary Fig. 14).

269 **Discussion**

270 Despite the substantial literature published on SARS-CoV-2, the molecular
271 mechanisms underpinning positive versus negative clinical outcomes remain poorly
272 defined. In this study, we examined the differences in circulating inflammatory
273 markers and metabolites in sera, and the composition of the gut microbiota, in a
274 large group of hospitalised patients with COVID-19. We have identified several
275 potential regulatory nodes whereby integrated immune, metabolic and microbiome
276 processes contribute to susceptibility or resilience to SARS-CoV-2 infection
277 associated damage.

278 Our identification of circulating inflammatory mediators that associate with
279 COVID-19 disease severity such as CRP and IL-6 are consistent with previous
280 reports and support the hypothesis that an overly aggressive immune response
281 contributes to immunopathology and severity^{28,29}. In addition to severity associated
282 factors, we have identified a subset of eight cytokines that are further dysregulated in
283 severe patients with a fatal outcome. Higher levels of IP-10 and IL-15 indicate
284 greater activation of a T helper 1 (Th1)-associated innate anti-viral response, while a
285 significant reduction in MDC levels may reflect the inhibitory effect of a Th1
286 environment on Th2 cytokines such as MDC. We were particularly interested in
287 TSLP as this cytokine is an epithelial cell-derived alarmin, which is released by
288 injured stromal cells to recruit and activate innate immune cells, and its blockade is
289 currently being investigated in asthma clinical studies^{30,31,32}. In combination with the
290 chemokines MCP-1 and IL-8, and ICAM-1 (which modulates leukocyte adhesion
291 and migration across endothelial cells), elevated TSLP levels indicate a greater
292 amount of epithelial tissue damage and inflammatory cell recruitment to the
293 damaged sites in patients who do not recover from SARS-CoV-2 infection. As

294 SARS-CoV-2 is a lytic virus, it is possible that viral replication in epithelial cells may
295 directly drive TSLP levels in sera, although indirect effects on epithelial cells within
296 the respiratory tract or gut might also induce TSLP release. Importantly, TSLP levels
297 were previously shown to be elevated in patients with long COVID, suggesting that
298 long term impacts of SARS-CoV-2 on epithelial cells should be examined in more
299 detail, potentially guiding future therapeutic interventions³³.

300 Significant metabolic reprogramming and compensatory responses are
301 evident in COVID-19 patients with severe disease and particularly in those with a
302 fatal outcome. Decreased serum levels of plasmalogens suggest a significant level
303 of systemic oxidative stress as these sacrificial phospholipids are preferentially
304 oxidised to protect more vulnerable membrane lipids such as polyunsaturated fatty
305 acids³⁴. Altered tryptophan metabolism was particularly interesting to observe as the
306 profound shutdown in serotonin production coupled with accumulation of quinolinic
307 acid indicated a shift from production of neuroprotective compounds to production of
308 neurotoxic compounds, which might be clinically relevant³⁵. An imbalance between
309 host and microbial tryptophan metabolism was also evident as serum kynurenine
310 levels increased, while products of bacterial tryptophan metabolism such as
311 indoleacetic acid were significantly decreased in those with severe and fatal
312 disease³⁶. These are important AhR ligands that can contribute to immune regulatory
313 responses, can drive an “exhaustion” phenotype in immune effector cells, and are
314 important for maintenance of the gut epithelial barrier by induction of IL-22^{37,38}. Other
315 significantly different metabolites such as the polyamines putrescine and spermidine
316 play important roles in protecting against inflammatory responses within the
317 airways³⁹. In addition, changes in secondary bile acid serum levels indicate
318 significant disruption of microbial metabolism and/or changes in the gut barrier.

319 Secondary bile acids significantly impact regulatory and effector immune responses,
320 which may be relevant for the development of severe COVID-19^{40,41}. Increased
321 levels of sulfonated bile acids in serum also indicates significant disruption of bile
322 acid metabolism in severely ill COVID-19 patients as sulfonation is an important
323 detoxification mechanism that prevents reabsorption of bile acids from the gut and
324 promotes their elimination in faeces⁴².

325 We identified a high-risk gut microbiome configuration associated with an
326 inflamed host phenotype and increased risk of the worst disease outcomes. Several
327 pathobionts including *Enterococcus* were enriched in severe disease, while well
328 described immune regulatory microbes such as *Bifidobacterium* and *Ruminococcus*
329 were enriched in those who survived^{43,44}. Similar microbiome configurations have
330 been described in other settings such as increasing age, whereby a decrease of the
331 core protective microbiome accompanied by an increase of pathobionts was
332 observed⁴⁵. In addition, acquisition of this subset of disease-associated taxa have
333 been shown to shift the metabolic state to a disease-like state²⁷. These changes in
334 the microbiome may have happened gradually over time and could potentially make
335 the host less resilient to SARS-CoV-2 infection.

336 The hyper-inflammatory state observed in COVID-19 patients with a fatal
337 outcome implies a failure in the negative feedback mechanisms that should restrain
338 the devastating overproduction of inflammatory cytokines and soluble mediators,
339 which lead to multiorgan failure. Our integrated analysis of microbiome features,
340 cytokines and metabolites suggests that important microbial-derived
341 immunoregulatory processes that contribute to negative feedback mechanisms may
342 be lacking in those with the most severe outcomes to SARS-CoV-2 infection.
343 Alternatively, increased levels of proinflammatory pathobionts may drive excessive

344 proinflammatory responses that cannot be contained by the regular feedback
345 mechanisms. While further studies will be required to determine causal interactions,
346 this study supports the hypothesis that successful responses to infectious agents
347 such as SARS-CoV-2 involve the gut microbiome mediated by effects on metabolism
348 and host inflammatory processes.

349 **Methods**

350 *Study Cohort*

351 We performed an investigator-initiated, prospective multicentre cohort study of adult
352 (≥ 18 years) patients who were admitted with Severe Acute Respiratory Syndrome
353 Coronavirus 2 (SARS-CoV-2) to four different hospitals in Switzerland and Ireland.
354 Infection was confirmed by SARS-CoV-2 polymerase-chain reaction (PCR) from an
355 upper or lower respiratory specimen. Exclusion criteria included COVID-19 diagnosis
356 after discharge from the ICU. Recruitment started in August 2020 and in total we
357 recruited 172 hospitalised patients from St. Gallen, Switzerland (n=37), Geneva,
358 Switzerland (n=50), Ticino, Switzerland (n=77) and Cork, Ireland (n=8). All patients
359 or patient representatives signed a patient informed consent. The study was
360 approved by local ethics committees (EKOS 20/058 for the three Swiss sites and
361 The Clinical Research Ethics Committee of the Cork Teaching Hospitals for Cork
362 University Hospital). Patients were enrolled typically within 24-48 h after admission to
363 the intensive care unit (ICU) or a hospital ward. Baseline characteristics, underlying
364 comorbidities and medication use at the time of sampling were collected and are
365 summarised in Table 1. All medical procedures and treatments were left at the
366 discretion of the treating physicians but documented in the database such as
367 complications during ICU stay and outcomes until hospital discharge. Patients were
368 categorised to have mild disease when there were no radiographic indications of
369 pneumonia and moderate disease if pneumonia with fever and respiratory tract
370 symptoms were present. Severe disease was defined as a respiratory rate ≥ 30
371 breaths per minute, oxygen saturation $\leq 93\%$ when breathing ambient air or
372 $\text{PaO}_2/\text{FiO}_2 \leq 300$ mm Hg, or anyone that required mechanical ventilation. Only those
373 that died during their hospital stay were recorded as a SARS-CoV-2-related death in

374 this study. Serum and faecal samples were collected as soon as possible following
375 enrolment into the study and immediately stored frozen at -80C at the clinical site.

376

377 *Cytokine Analysis*

378 We examined the levels of 54 cytokines and growth factors (using MSD
379 multiplex kits according to manufacturer's instructions) in the serum of 172
380 hospitalised COVID-19 patients. Serum from patients was typically obtained within
381 24 hours after study enrolment. Sera obtained prior to the pandemic from 29 healthy
382 volunteers were analysed in parallel. The mediators measured included IL-1 α , IL-1 β ,
383 IL-1RA, IL-2, IL-3, IL-4, IL-5, IL-6, IL-7, IL-8, IL-9, IL-10, IL-12/23p40, IL-12p70, IL-
384 13, IL-15, IL-16, IL-17A, IL-17A/F, IL-17B, IL-17C, IL-21, IL-22, IL-23, IL-27, IL-31,
385 TNF- α , TNF- β , IFN- γ , IP-10, MIP-1 α , MIP-1 β , MIP-3 α , MCP-1, MCP-4, Eotaxin,
386 Eotaxin-3, TARC, MDC, TSLP, CRP, SAA, VEGF-A, VEGF-C, VEGF-D, sTie-2, Flt-
387 1, sICAM-1, sVCAM-1, bFGF, PlGF and GM-CSF.

388

389 *Metabolomics*

390 Untargeted metabolomics on patient sera was performed by MetabolonTM
391 using the HD4 platform. Briefly, all methods utilized a Waters ACQUITY ultra-
392 performance liquid chromatography (UPLC) and a Thermo Scientific Q-Exactive high
393 resolution/accurate mass spectrometer interfaced with a heated electrospray
394 ionization (HESI-II) source and Orbitrap mass analyzer operated at 35,000 mass
395 resolution. The sample extract was dried then reconstituted in solvents compatible
396 to each of the four methods. One aliquot was analyzed using acidic positive ion
397 conditions, chromatographically optimized for more hydrophilic compounds. Another
398 aliquot was also analyzed using acidic positive ion conditions, however it was

399 chromatographically optimized for more hydrophobic compounds. Another aliquot
400 was analyzed using basic negative ion optimized conditions using a separate
401 dedicated C18 column. The fourth aliquot was analyzed via negative ionization
402 following elution from a HILIC column (Waters UPLC BEH Amide 2.1x150 mm, 1.7
403 μm) using a gradient consisting of water and acetonitrile with 10mM Ammonium
404 Formate, pH 10.8. The MS analysis alternated between MS and data-dependent
405 MSn scans using dynamic exclusion. The scan range varied slightly between
406 methods but covered 70-1000 m/z.

407

408 *16S sequencing*

409 Fecal samples were obtained as soon as possible following hospitalisation.
410 Total community DNA was extracted from fecal samples by a combined Repeat
411 Bead Beating - Qiagen DNA extraction method, and the V3 dash V4 region of the
412 16S gene was amplified and sequenced as previously described⁴⁶. The uniquely
413 barcoded amplicons were sequenced on an Illumina MiSeq platform (Illumina,
414 California, USA) utilizing 2x300 bp chemistry.

415

416 *Bioinformatic analysis*

417 From the Log2 transformed metabolomics data obtained from Metabolon, any
418 metabolite with no variance among samples was removed. Pairwise differential
419 abundance analysis was performed between conditions using R package LIMMA.
420 Benjamini-Hochberg correction (BH) was applied for each comparison. R packages
421 Boruta was applied for feature and tree number selection before random forest
422 analysis. Random forest classifiers were built with the most important features, 1000
423 trees, mtry of 1 and 10-fold cross-validation using R packages caret and

424 randomForest. They were evaluated using confusion matrices/roc curves. For
425 association analysis, significant positive correlations (Spearman, FDR<0.0005) were
426 extracted and used to build the network using python igraph
427 (<https://igraph.org/python/>). The strength of the connections and relevance of the
428 network was evaluated by plotting distribution of correlation coefficients and
429 comparison of the network to a random network with similar dimensions. Community
430 detection was performed using the Leiden algorithm from the python module
431 leidenalg (<https://leidenalg.readthedocs.io/en/stable/index.html>). For each community
432 large enough (N>30), metabolite set enrichment analysis (MSEA) was performed.
433 For metabolite set enrichment analysis (MSEA), all Metabolon™ terms were
434 extracted with their corresponding metabolites as reference. Python 3 gseapy
435 package was used to perform a hypergeometric test between list of significant
436 metabolites and reference. Importance plots, dot plots, bar plots, pca plots were
437 produced with R package ggplot2. Heatmaps were designed with the R package
438 ComplexeHeatmap. Networks were represented using Cytoscape 3.6.1 and
439 metabolites of interest highlighted.

440 For the microbiome analysis, the raw Illumina reads obtained for each sample
441 were quality-filtered using the trimmomatic program, using the default parameters⁴⁷.
442 The quality filtered reads were then taxonomically classified using both DADA2⁴⁸ (for
443 read-level genus classification and identification of amplicon sequence variants or
444 ASVs within each sample) and Spingo⁴⁹ (for species level classification). Amplicon
445 Sequence Variants obtained using DADA2 for all the samples were then further
446 merged by performing into Operational Taxonomic Units (OTUs) using the denovo-
447 sequence-based clustering using the qiime⁵⁰ package.

448 Subsequent downstream analyses of the taxonomic profiles (at all three
449 levels, namely genus, species and OTU) as well as integrated analysis of taxonomic
450 profiles with cytokine profiles and the metabolome were performed using various
451 modules/packages of the R programming interface (v 4.0.3; R Core Team 2020).
452 Estimates of alpha diversity were computed using the diversity function of the vegan
453 package of R. Principal Coordinate Analyses (PCoA) were computed using the ade4
454 package. The envfit function of the vegan package was used to perform the envfit-
455 based analysis using the three top Principal Coordinates. Enterotyping of the gut
456 microbiome profiles was performed as described in a previous study from our
457 group⁵¹. Two group comparison of microbiome abundances were performed using
458 the Mann-Whitney tests (using the wilcox.test function of R stats package. For more
459 than two-group comparisons, pairwise comparisons within groups were computed
460 using Mann-Whitney tests. The p-values were corrected using Benjamini-Hochberg
461 FDR correction (p.adjust function of the stats package). Ordinary Least Squares
462 (OLS) regression after adjusting for confounders were performed using the glm
463 function of the stats package.

464 Correlation analysis of associations amongst features in three data layers
465 (genus-level microbiome, metabolome and cytokine profiles) were performed using
466 the Weighted Gene-Coexpression Network Analysis (WGCNA)⁵². While originally
467 devised for computing gene co-expression networks, WGCNA is now being used in
468 studies to integrate data from multiple OMICs layers^{53,54}. In this study, the WGCNA
469 was performed using an optimal soft-power threshold of 7 for scale-free topology.
470 Using hierarchical clustering and topology overlap measures (TOM), we identified
471 that the features from the three data layers could be optimally grouped into 14
472 modules, which were then investigated for association with disease symptoms using

473 OLS models. The association networks within each module were then computed
474 using the ReBoot approach as implemented in the ccrepe workflow⁵⁵.

475

476 **Acknowledgements**

477 The authors are supported in part by Science Foundation Ireland (SFI) in the
478 form of a research center grant to APC Microbiome Ireland (12/RC/2273_P2) and
479 two COVID-RRC awards (20/COV/0158 (LOM) and 20/COV/0125 (PWOT)). Work in
480 UN's laboratory is supported by the Swedish Research Council grants (2017-01330
481 and 2018-06156). In addition, funding from an Intramural grant, Cantonal Hospital St.
482 Gallen, Fondazione Leonardo and Fondazione Metis Mantegazza supported this
483 study.

484 For their valuable contributions to this study, we would like to thank Susan
485 Rafferty-McArdle, Mary Crowley, Manasi Nadkarni, John MacSharry, Liam Fanning,
486 Brian McSharry (University College Cork); Ines Thiele (University College Galway);
487 Christian Kahlert, Miodrag Filipovic, Cornelia Knapp, Susanne Nigg, Thomas Egger,
488 Andrea Blöchlinger, Tia Wisser, Melanie Gätzi and Patrick Mürger (Cantonal
489 Hospital St. Gallen); Kenza Bouras, Aurélie Perret and Philippe Montillier (Geneva
490 University Hospitals and the University of Geneva Faculty of Medicine); Maurizia
491 Bissig-Canevascini and Claudia Di Bartolomeo (Fondazione Epatocentro Ticino).

492

493

494 **Table 1. Patient Demographics**

	Healthy Controls	Mild/Moderate	Severe - Survivors	Severe-Fatal
495				
496	n= 29	42	89	41
497	Age (S.D.) ^{1,2} 45.3 (10.1)	58.0 (15.7)	65.0 (11.2)	69.1 (8.7)
498	Male/Female ² 16/13	16/26	72/17	32/9
499	BMI (S.D.) ² 26.9 (5.7)	24.4 (4.1)	28.2 (5.6)	27.6 (5.5)
500	Obese (BMI > 30) ² 20%	14%	35%	34%
501				
502	<i>Medications at First Sampling Timepoint</i>			
503	PPI ² 0%	20%	55%	62%
504	Antibiotics ² 0%	16%	37%	40%
505	Immunosuppressives ² 0%	20%	61%	65%
506				
507	<i>Pre-existing Comorbidities</i>			
508		Hypertension 34%	49%	45%
509		Dyslipidemia ² 9%	24%	30%
510		Diabetes 17%	22%	25%
511		Respiratory – COPD/Asthma 20%	8%	15%
512		Chronic Kidney Disease 3%	4%	8%
513		Previous Neoplasia 20%	15%	22%
514				
515	=====			
516	=====			

517 ¹p<0.05 Healthy Controls versus all COVID-19 Patients

518 ²p<0.05 Mild/Moderate versus Severe COVID-19

519 PPI – Pantoprazole; Omeprazole

520 Antibiotics – Amoxicillin; Azithromycin; Sulfamethoxazole; Clarithromycin

521 Immunosuppressives – Dexamethasone; Methylprednisolone; Prednisolone

522

523

524 **Figure Legends.**

525 *Fig.1 Circulating immune mediators in COVID-19 patients.*

526 a) PCA plot illustrating the differences in serum cytokine and inflammatory mediator
527 levels in COVID-19 patients with different levels of severity. b) Heatmap illustrates
528 the serum immune mediators that are significantly increased (red), significantly
529 decreased (blue), or remain unchanged (green). c) Levels of the cytokines that are
530 significantly different in patients with severe COVID-19 that survive (labelled
531 “Severe”), compared to those with severe COVID-19 that have a fatal outcome
532 (labelled “Fatal”). Differences between groups are calculated using the Kruskal-
533 Wallis test and Dunn's multiple comparison test (* $p < 0.05$, ** $p < 0.01$, *** $p < 0.001$,
534 **** $p < 0.0001$).

535

536 *Fig. 2. Serum metabolites in COVID-19 patients.*

537 a) PCA plot for the four conditions: control, mild/moderate, severe, fatal; b) Barplot
538 representing super pathways of the significant metabolites (LIMMA, FDR<0.05)
539 between each comparison of conditions; c) Importance plot and confusion matrix
540 from the random forest classifier between the four conditions.

541

542 *Fig. 3. Serum metabolites in COVID-19 patients.*

543 a) Heatmap representing metabolites from pathways of interest, listed at the bottom
544 of the figure, divided according to group. Log fold change (LFC) for significant
545 pairwise comparisons (LIMMA, FDR<0.05) are included. Sulphonated bile acids and
546 metabolites of microbial origin are indicated. b) Weighted co-expression network
547 labelled for metabolites from pathways of interest. c) Pathway enrichment analysis
548 using Metabolon terms for communities 1, 3 and 5 (significant terms are displayed,

549 gseapy, FDR<0.2). d) Subset of metabolites of targeted pathways from co-
550 expression network analysis. e) Weighted co-expression network labelled for those
551 metabolites that were significantly different between severe COVID-19 patients that
552 survived versus those that died (LIMMA, FDR<0.05).

553

554 *Fig. 4. Gut microbiome composition in COVID-19 patients.*

555 (a) Principal coordinate analysis of the genus-level microbiome composition of the
556 three outcome groups of patients obtained using the Canberra distance measure. (b)
557 Variation of the silhouette-Scores obtained, across for cluster sizes (k), for 50
558 iterations of k-means clustering of the first three dominant Principal coordinates of
559 the genus-level microbiome profiles. The principal coordinates of these two
560 microbiome groups are demarcated in (c). The two microbiome groups exhibited
561 distinct patterns of association with three COVID-19 disease severity outcome
562 groups (d). Volcano plot illustrates genera showing either significant ($FDR \leq 0.15$,
563 shown in blue) or nominally significant ($P \leq 0.05$, shown in cyan) associations with
564 PCo1. The x-axis shows the estimate of the linear-regression models (direction
565 indicating the pattern of association) and y-axis shows the -logarithm of the p-value
566 to the base 10. The genera associating with the high-risk MicrobiomeGroup1 are on
567 the negative axis and those associating with low-risk MicrobiomeGroup2 are on the
568 positive axis. Only those genera showing associations with $P \leq 0.05$ are shown.

569

570 *Fig. 5. Modules that positively correlate with severe and fatal COVID-19.*

571 Feature-to-feature positive association networks obtained using the ccrepe approach
572 (Spearman correlations, 1000 iterations) for modules (or Module groups) that show
573 (a) significantly positive ('turquoise') and (b) significantly negative ('red', 'blue',

574 'yellow', and 'black') associations with severe and fatal COVID-19. In (b) given the
575 presence of features from four different modules, the location of the features
576 belonging to the different modules are indicated in the smaller network
577 representation in the lower left-hand corner. Microbiome, cytokine and metabolite
578 features that are associated with severity and death are highlighted in different
579 colours.

580 **Supplementary Figure Legends**

581 *Supplementary Fig. 1. Serum cytokine levels.*

582 Differences between groups are calculated using the Kruskal-Wallis test and Dunn's
583 multiple comparison test (* $p < 0.05$, ** $p < 0.01$, *** $p < 0.001$, **** $p < 0.0001$).

584

585 *Supplementary Fig. 2. Metabolite set enrichment analysis.*

586 Using Metabolon terms (gseapy, FDR < 0.2), bubble size represents the number of
587 metabolites found in each pathway. Color is specific to each comparison.

588

589 *Supplementary Fig. 3. Random forest analysis of serum metabolites.*

590 The metabolite features and AUC curves for random forest analysis of COVID-19
591 patients with mild/moderate disease compared to those with severe disease (a);
592 COVID-19 patients with a fatal outcome compared to those with mild/moderate
593 disease (b); COVID-19 patients that survive following severe disease compared to
594 those that don't survive following severe disease (c).

595

596 *Supplementary Fig. 4. Serum microbial metabolites.*

597 Representative examples of metabolites generated by host metabolism of tryptophan
598 (a). Selected examples of serum levels of microbial metabolites due to tryptophan
599 metabolism (b) or SCFAs (c). Serum citrulline levels (d). PCA plot illustrates the
600 differences in serum metabolites associated with microbial metabolism (e).

601 Differences between groups are calculated using the Kruskal-Wallis test and Dunn's
602 multiple comparison test (* $p < 0.05$, ** $p < 0.01$, **** $p < 0.0001$).

603

604 *Supplementary Fig. 5. Gut microbiome alpha diversity.*

605 Boxplots showing the variation of the Shannon Diversity and Detected taxa for the
606 gut microbiome profiles for the three outcome groups at OTU (a and d), Species (b
607 and e) and Genus (c and f) levels.

608

609 *Supplementary Fig. 6. Gut microbiome beta diversity.*

610 Principal coordinate analysis showing the resolution of the gut microbiome profiles
611 from the 99 patients belonging to the three outcome groups at (a) OTU and (b)
612 Species level, obtained using four different distance measures. (c) Principal
613 coordinate analysis showing the resolution of the gut microbiome profiles from the 99
614 patients belonging to the three outcome groups at the genus level obtained using the
615 Spearman, Bray-Curtis and Jaccard distance measures.

616

617 *Supplementary Fig. 7. Cytokine levels associated with Microbiome Groups.*

618 Boxplot showing the differences in the cumulated range-scaled levels of the three
619 groups of elevated cytokines between surviving patients with severe symptoms who
620 had a high-risk MicrobiomeGroup1 and those patients with severe symptoms who
621 were classified to the low-risk MicrobiomeGroup2. The p-values of the Mann-
622 Whitney tests obtained for the comparisons within the three groups of cytokines are
623 indicated. Each cytokine level was range-scaled across patients to a value between
624 0 and 1. For each patient, the range-scaled values of all cytokines within the same
625 group were then cumulated by adding the corresponding range-scaled values
626 obtained for the given patient.

627

628 *Supplementary Fig. 8. Bacterial genera correlate with circulating inflammatory*
629 *mediators.*

630 Heatmap showing the Spearman correlations between the 73 genus-level markers
631 (detected in at least 5 of the 99 patients and showing association with $FDR \leq 0.15$
632 with at least one of the severity/fatality-associated cytokines) and 28 severity/fatality-
633 associated cytokines. The groups of the different cytokines and their direction of
634 change (elevated or reduced) with severity/fatality are also indicated in specific
635 colors. Also indicated are the patterns of the various genus-level markers with PCo1
636 that resolves the two microbiome groups (positive PCo1 with MicrobiomeGroup2).
637 The genera whose associations are indicated in red boxes are those that did not
638 show any associations with either of the two Microbiome configurations (or groups)
639 in terms of their association with PCo1, but independently show association with an
640 inflamed host phenotype. The genera in green boxes show the opposite trends with
641 the inflamed phenotype.

642

643 *Supplementary Figure 9. Overview of the steps and the results of combined WGCNA*
644 *from the three data layers.*

645 (A) shows the Scaled-Independence plot and the Scale-free topology fit and
646 highlights the selection of the soft-power of 7 as it has the maximum scale-free
647 nature for the network. (B) Shows the regression coefficients of the 14 modules
648 obtained using Ordinary Least-square Regression for worse outcome (where in the
649 outcomes were ranked as 1 for mild and moderate; 2 for severe and 3 for death).
650 The modules with significant (Benjamini-Hochberg corrected $FDR \leq 0.05$) and
651 nominal associations ($P \leq 0.05$) are also indicated. (C) Shows the sizes of the
652 different modules in terms of the feature

653

654 *Supplementary Fig. 10. Modules showing nominal positive associations with severity*
655 *and death.*

656 Positive association networks obtained for the features affiliated to (a) brown and (b)
657 the tan module, using the ccrepe approach (Spearman correlation, iterations = 1000,
658 $p \leq 0.01$). Key taxa and metabolites are highlighted.

659

660 *Supplementary Fig. 11. Association patterns within the 'red' module.*

661 Positive association networks obtained for the features affiliated to the red module,
662 using the ccrepe approach (Spearman correlation, iterations = 1000, $p \leq 0.01$). Key
663 taxa and metabolites are highlighted.

664

665 *Supplementary Fig. 12. Association patterns within the 'blue module.*

666 Positive association networks obtained for the features affiliated to the blue module,
667 using the ccrepe approach (Spearman correlation, iterations = 1000, $p \leq 0.01$). Key
668 taxa and metabolites are highlighted.

669

670 *Supplementary Fig. 13. Association patterns within the 'black' module.*

671 Positive association networks obtained for the features affiliated to the black module,
672 using the ccrepe approach (Spearman correlation, iterations = 1000, $p \leq 0.01$). Key
673 taxa and metabolites are highlighted.

674

675 *Supplementary Fig. 14. Association patterns within the 'yellow module.*

676 Positive association networks obtained for the features affiliated to the yellow
677 module, using the ccrepe approach (Spearman correlation, iterations = 1000, $p \leq$
678 0.01). Key taxa and metabolites are highlighted.

679 **References**

- 680 1. Huang, C. et al. Clinical features of patients infected with 2019 novel coronavirus
681 in Wuhan, China. *Lancet* **395**, 497–506 (2020).
- 682 2. Williamson, E. J. et al. Factors associated with COVID-19-related death using
683 OpenSAFELY. *Nature* **584**, 430–436 (2020).
- 684 3. Bastard, P. et al. Autoantibodies against type I IFNs in patients with life-
685 threatening COVID-19. *Science* **370**, eabd4585 (2020).
- 686 4. Sokolowska, M. et al. Immunology of COVID-19: Mechanisms, clinical outcome,
687 diagnostics, and perspectives-A report of the European Academy of Allergy and
688 Clinical Immunology (EAACI). *Allergy* **75**, 2445-2476 (2020).
- 689 5. Azkur, A.K. et al. Immune response to SARS-CoV-2 and mechanisms of
690 immunopathological changes in COVID-19. *Allergy* **75**, 1564-1581 (2020).
- 691 6. Radzikowska, U. et al. Distribution of ACE2, CD147, CD26, and other SARS-CoV-
692 2 associated molecules in tissues and immune cells in health and in asthma, COPD,
693 obesity, hypertension, and COVID-19 risk factors. *Allergy* **75**, 2829-2845 (2020).
- 694 7. Overmyer, K.A. et al. Large-Scale Multi-omic Analysis of COVID-19 Severity. *Cell*
695 *Syst.* **12**, 23-40 (2021).
- 696 8. Giron, L.B. et al. Plasma Markers of Disrupted Gut Permeability in Severe COVID-
697 19 Patients. *Front Immunol.* **12**, 686240 (2021).
- 698 9. Blanco-Melo, D. et al. Imbalanced Host Response to SARS-CoV-2 Drives
699 Development of COVID-19. *Cell* **181**, 1036-1045 (2020).
- 700 10. Norooznezhad, A.H. & Mansouri, K. Endothelial cell dysfunction, coagulation,
701 and angiogenesis in coronavirus disease 2019 (COVID-19). *Microvasc Res.* **137**,
702 104188 (2021).

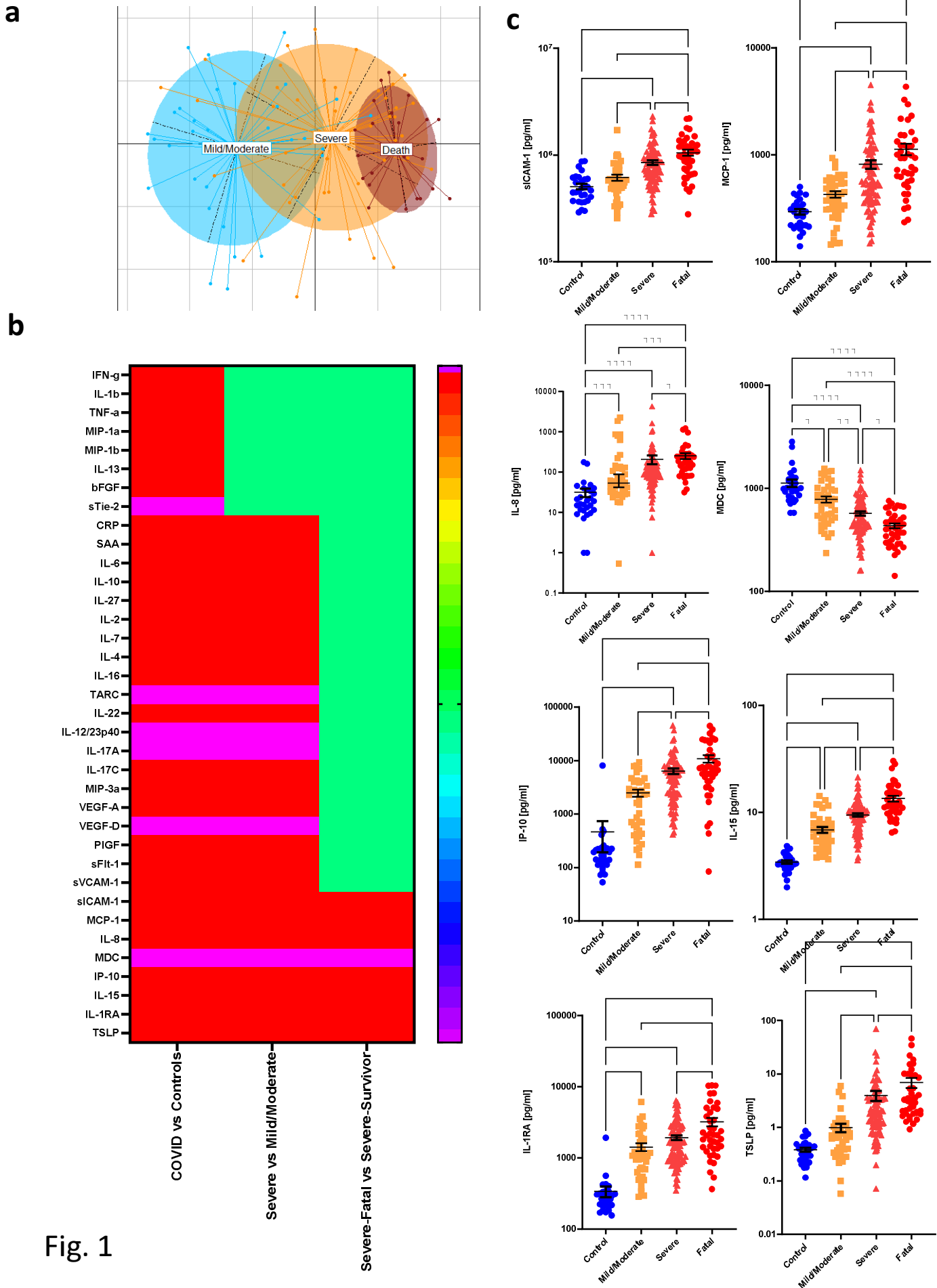
- 703 11. Sumbria, D., Berber, E., Mathayan, M. & Rouse, B.T. Virus Infections and Host
704 Metabolism-Can We Manage the Interactions? *Front Immunol.* **11**, 594963 (2021).
- 705 12. Groeger, D. et al. Intranasal Bifidobacterium longum protects against viral-
706 induced lung inflammation and injury in a murine model of lethal influenza infection.
707 *EBioMedicine.* **60**, 102981 (2020).
- 708 13. Stefan, K. L., Kim, M. V., Iwasaki, A. & Kasper, D. L. Commensal microbiota
709 modulation of natural resistance to virus infection. *Cell* **183**, 1312–1324 (2020).
- 710 14. Yeoh, Y.K. et al. Gut microbiota composition reflects disease severity and
711 dysfunctional immune responses in patients with COVID-19. *Gut* **70**, 698-706 (2021).
- 712 15. Smith, N. et al. Distinct systemic and mucosal immune responses during acute
713 SARS-CoV-2 infection. *Nat Immunol* 2021 Sep 1. doi: 10.1038/s41590-021-01028-7.
- 714 16. Lunjani, N., Ahearn-Ford, S., Dube, F.S., Hlela, C. & O'Mahony, L. Mechanisms
715 of microbe-immune system dialogue within the skin. *Genes Immun* 2021 May 15.
716 doi: 10.1038/s41435-021-00133-9.
- 717 17. Michalovich, D., et al. Obesity and disease severity magnify disturbed
718 microbiome-immune interactions in asthma patients. *Nat Commun* **10**, 5711 (2019).
- 719 18. Akdis, C.A. Does the epithelial barrier hypothesis explain the increase in allergy,
720 autoimmunity and other chronic conditions? *Nat Rev Immunol.* 2021 Apr 12. doi:
721 10.1038/s41577-021-00538-7.
- 722 19. Tsai, Y.W. et al. Gut Microbiota-Modulated Metabolomic Profiling Shapes the
723 Etiology and Pathogenesis of Autoimmune Diseases. *Microorganisms* **9**, 1930
724 (2021).
- 725 20. Wastyk, H.C. et al. Gut-microbiota-targeted diets modulate human immune
726 status. *Cell* **184**, 4137-4153 (2021).

- 727 21. Liwinski, T., Zheng, D. & Elinav, E. The microbiome and cytosolic innate immune
728 receptors. *Immunol Rev.* **297**, 207-224 (2020).
- 729 22. Barcik, W., Wawrzyniak, M., Akdis, C.A. & O'Mahony, L. Immune regulation by
730 histamine and histamine-secreting bacteria. *Curr Opin Immunol.* **48**, 108-113 (2017).
- 731 23. Hosseinkhani, F. et al. The contribution of gut bacterial metabolites in the human
732 immune signaling pathway of non-communicable diseases. *Gut Microbes* **13**, 1-22
733 (2021).
- 734 24. Bar, N. et al. A reference map of potential determinants for the human serum
735 metabolome. *Nature* **588**, 135-140 (2020).
- 736 25. Krishnan, S. et al. Metabolic perturbation associated with COVID-19 disease
737 severity and SARS-CoV-2 replication. *Mol Cell Proteomics* **Oct 4**, 100159 (2021).
- 738 26. Shanahan, F., Ghosh, T.S. & O'Toole, P.W. The Healthy Microbiome-What Is the
739 Definition of a Healthy Gut Microbiome? *Gastroenterology* **160**, 483-494 (2021).
- 740 27. Ghosh, T.S., Das, M., Jeffery, I.B. & O'Toole, P.W. Adjusting for age improves
741 identification of gut microbiome alterations in multiple diseases. *Elife* **9**, e50240
742 (2020).
- 743 28. Lucas, C. et al. Longitudinal analyses reveal immunological misfiring in severe
744 COVID-19. *Nature* **584**, 463–469 (2020).
- 745 29. Mathew, D. et al. Deep immune profiling of COVID-19 patients reveals distinct
746 immunotypes with therapeutic implications. *Science* **369**, eabc8511 (2020).
- 747 30. Roan, F., Obata-Ninomiya, K. & Ziegler, S.F. Epithelial cell-derived cytokines:
748 more than just signaling the alarm. *J Clin Invest* **129**, 1441–1451 (2019).
- 749 31. Corren, J. & Ziegler, S.F. TSLP: From Allergy to Cancer. *Nat Immunol* **20**, 1603–
750 1609 (2019).

- 751 32. Corren, J. et al. Tezepelumab in adults with uncontrolled asthma. *N Engl J Med*
752 **377**, 936–946 (2017).
- 753 33. Ahearn-Ford, S. et al. Long-term disruption of cytokine signalling networks is
754 evident in patients who required hospitalization for SARS-CoV-2 infection. *Allergy*
755 **76**, 2910-2913 (2021).
- 756 34. Braverman, N.E. & Moser, A.B. Functions of plasmalogen lipids in health and
757 disease. *Biochim Biophys Acta* **1822**, 1442-1452 (2012).
- 758 35. Modoux, M., Rolhion, N., Mani, S. & Sokol, H. Tryptophan Metabolism as a
759 Pharmacological Target. *Trends Pharmacol Sci* **42**, 60-73 (2021).
- 760 36. Whitehead, T.R., Price, N.P., Drake, H.L. & Cotta, M.A. Catabolic Pathway for
761 the Production of Skatole and Indoleacetic Acid by the Acetogen Clostridium
762 Drakei, Clostridium Scatologenes, and Swine Manure. *Appl Environ Microbiol* **74**,
763 1950–1953 (2008).
- 764 37. Gasaly, N., de Vos, P. & Hermoso, M.A. Impact of Bacterial Metabolites on Gut
765 Barrier Function and Host Immunity: A Focus on Bacterial Metabolism and Its
766 Relevance for Intestinal Inflammation. *Front Immunol* **12**, 658354 (2021).
- 767 38. Scott, S.A., Fu, J. & Chang, P.V. Microbial tryptophan metabolites regulate gut
768 barrier function via the aryl hydrocarbon receptor. *Proc Natl Acad Sci* **117**, 19376–
769 19387 (2020).
- 770 39. Wawrzyniak, M. et al. Spermidine and spermine exert protective effects within
771 the lung. *Pharmacol Res Perspect* **9**, e00837 (2021).
- 772 40. Campbell, C. et al. Bacterial Metabolism of Bile Acids Promotes Generation of
773 Peripheral Regulatory T Cells. *Nature* **581**, 475–479 (2020).
- 774 41. Hagan, T. et al. Antibiotics-Driven Gut Microbiome Perturbation Alters Immunity
775 to Vaccines in Humans. *Cell* **178**, 1313-1328 (2019).

- 776 42. Dawson, P.A. & Karpen, S.J. Intestinal transport and metabolism of bile acids. *J*
777 *Lipid Res* **56**, 1085-1099 (2015).
- 778 43. Konieczna, P., Akdis, C.A., Quigley, E.M., Shanahan, F. & O'Mahony, L. Portrait
779 of an immunoregulatory Bifidobacterium. *Gut Microbes* **3**, 261-266 (2012).
- 780 44. La Reau, A.J. & Suen, G. The Ruminococci: key symbionts of the gut ecosystem.
781 *J Microbiol* **56**, 199-208 (2018).
- 782 45. O'Toole, P.W. & Jeffery, I.B. Microbiome-health interactions in older people. *Cell*
783 *Mol Life Sci* **75**, 119-128 (2018).
- 784 46. McCarthy, S. et al. Altered Skin and Gut Microbiome in Hidradenitis Suppurativa.
785 *J Invest Dermatol* S0022-202X(21)01657-2 (2021).
- 786 47. Bolger, A.M., Lohse, M. & Usadel, B. Trimmomatic: a flexible trimmer for Illumina
787 sequence data. *Bioinformatics* **30**, 2114-2120 (2014).
- 788 48. Callahan, B.J. et al. DADA2: High-resolution sample inference from Illumina
789 amplicon data. *Nat Methods* **13**, 581-583 (2016).
- 790 49. Allard, G., Ryan, F.J., Jeffery, I.B. & Claesson, M.J. SPINGO: a rapid species-
791 classifier for microbial amplicon sequences. *BMC bioinformatics* **16**, 324 (2015).
- 792 50. Caporaso, J.G. et al. QIIME allows analysis of high-throughput community
793 sequencing data. *Nat Methods* **7**, 335-336 (2010).
- 794 51. Ghosh, T.S., Arnoux, J. & O'Toole, P.W. Metagenomic analysis reveals distinct
795 patterns of gut lactobacillus prevalence, abundance, and geographical variation in
796 health and disease. *Gut Microbes* **12**, 1-19 (2020).
- 797 52. Langfelder, P. & Horvath, S. WGCNA: an R package for weighted correlation
798 network analysis. *BMC Bioinformatics* **9**, 559 (2008).
- 799 53. Pei, G., Chen, L. & Zhang, W. WGCNA Application to Proteomic and
800 Metabolomic Data Analysis. *Methods Enzymol* **585**, 135-158 (2017).

- 801 54. Jeffery, I.B. et al. Differences in Fecal Microbiomes and Metabolomes of People
802 With vs Without Irritable Bowel Syndrome and Bile Acid Malabsorption.
803 *Gastroenterology* **158**, 1016-1028 (2020).
- 804 55. Faust, K. et al. Microbial co-occurrence relationships in the human microbiome.
805 *PLoS Comput Biol* **8**, e1002606 (2012).
- 806



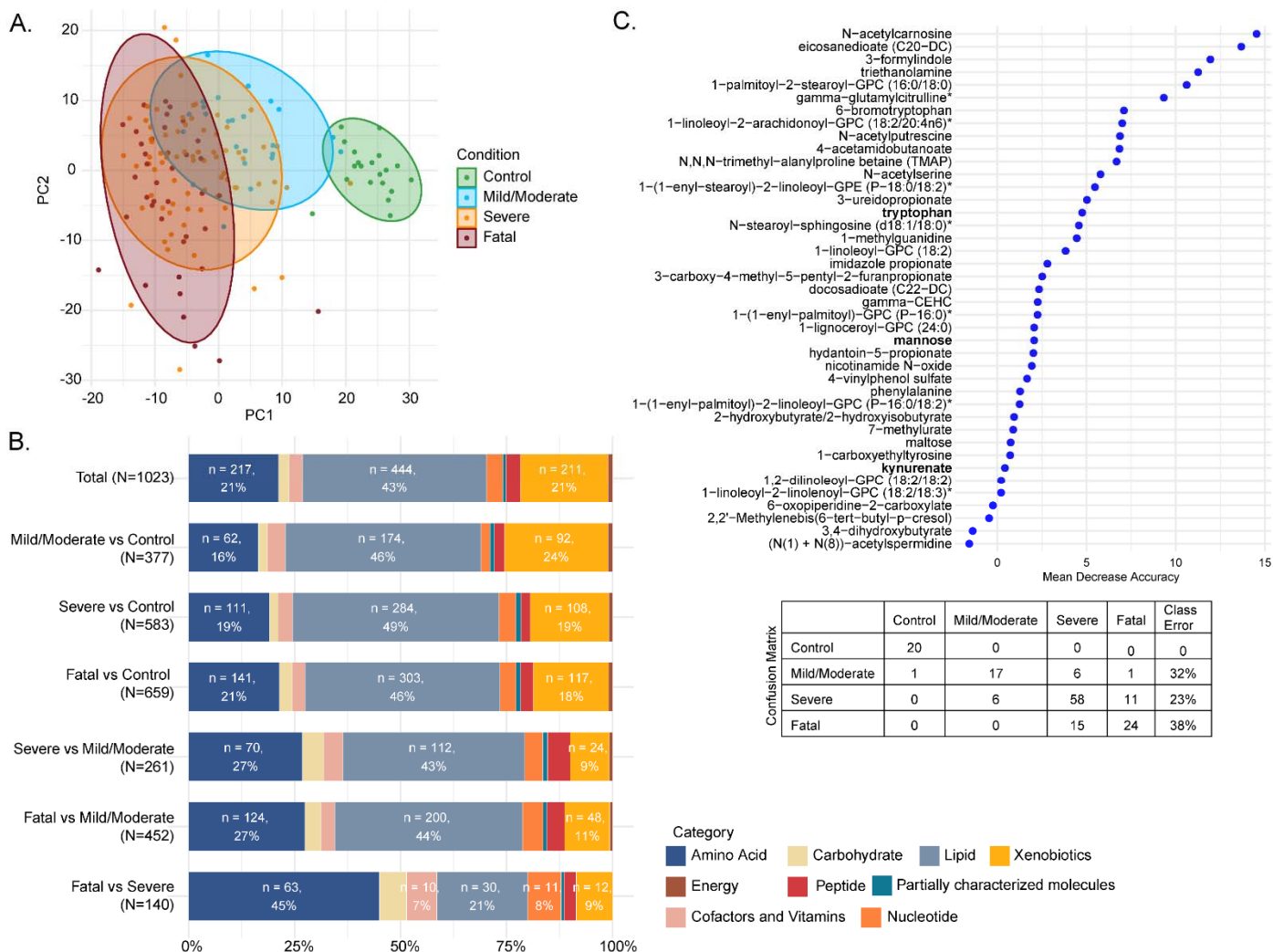


Fig. 2

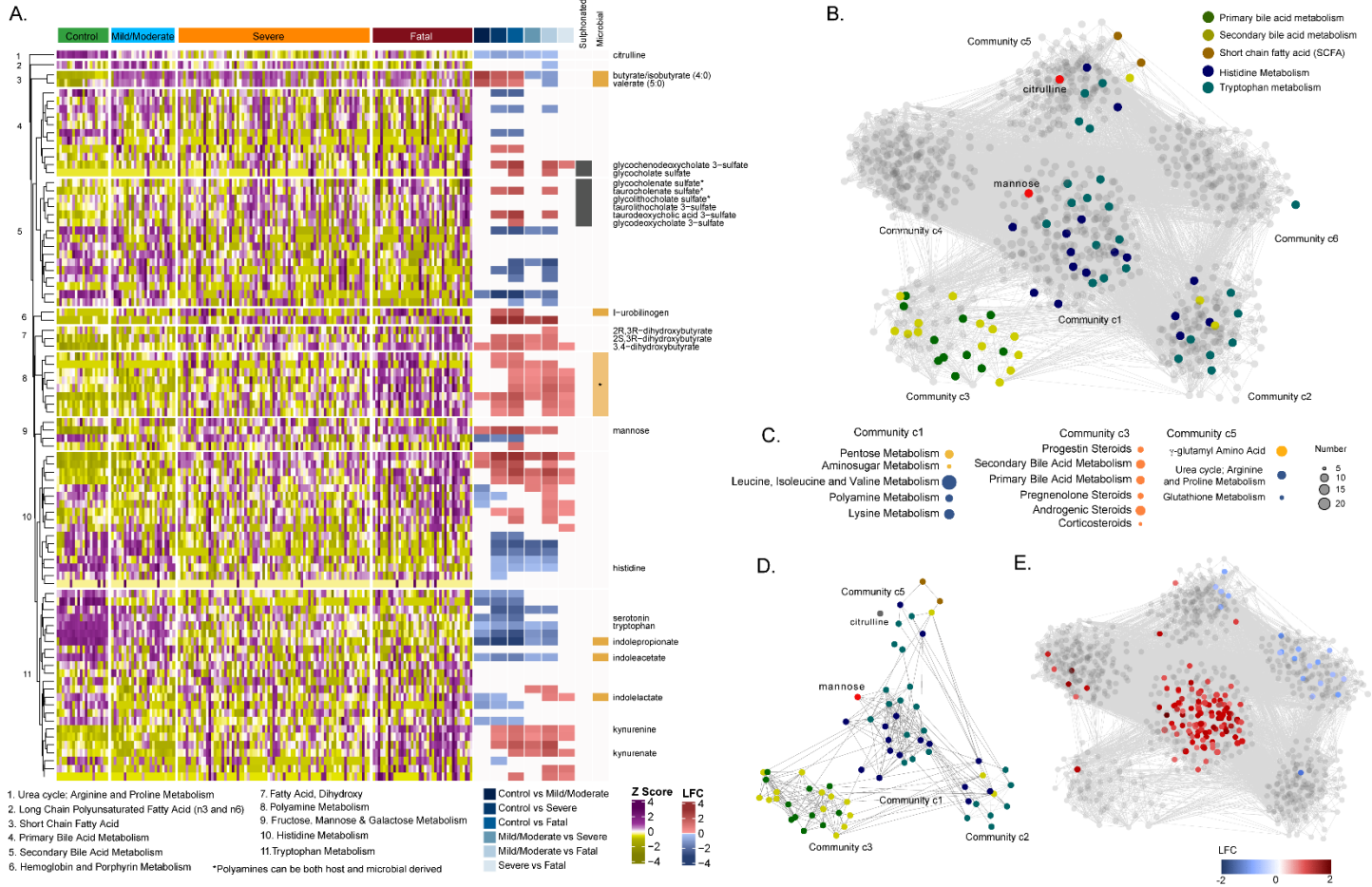
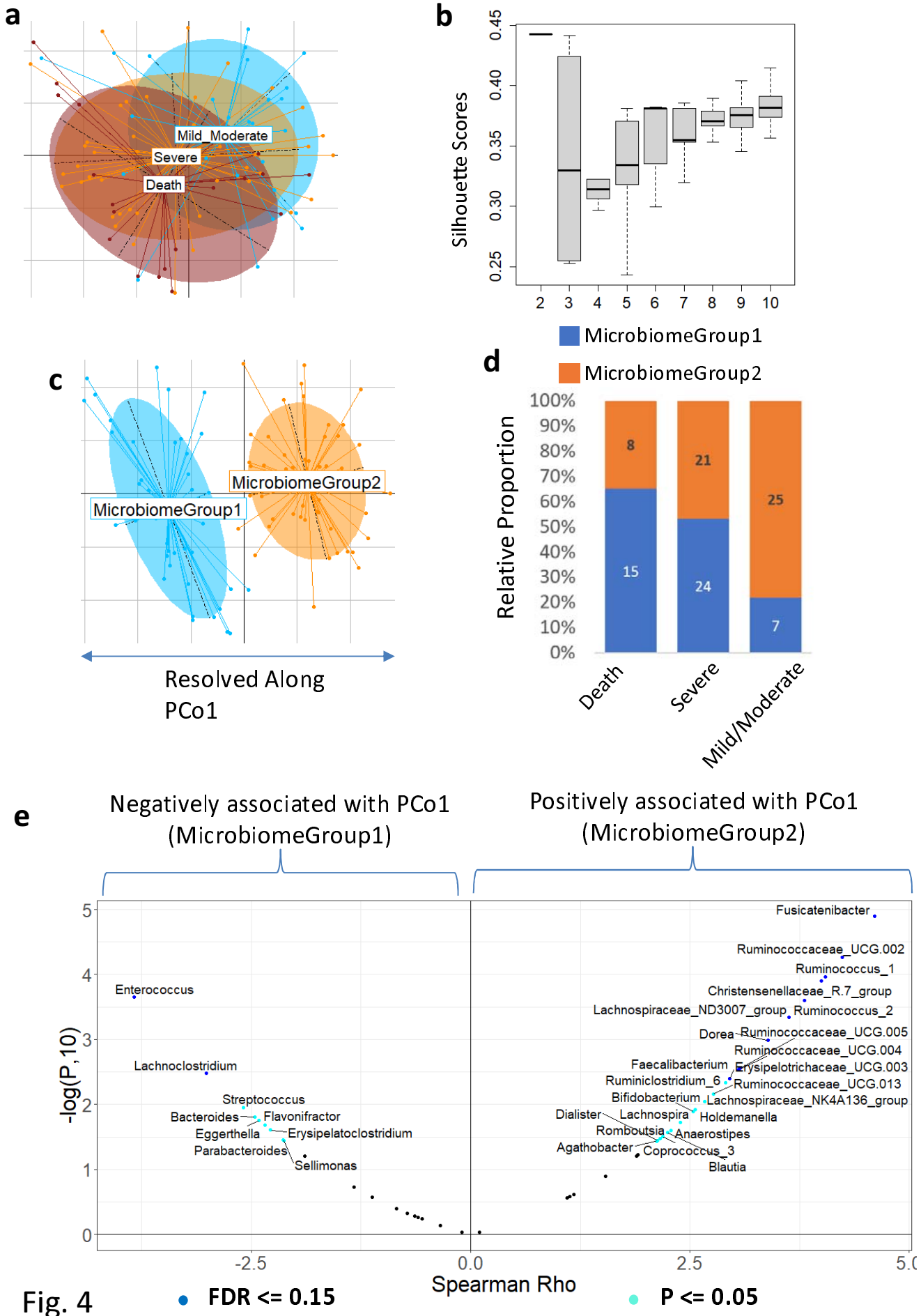


Fig. 3



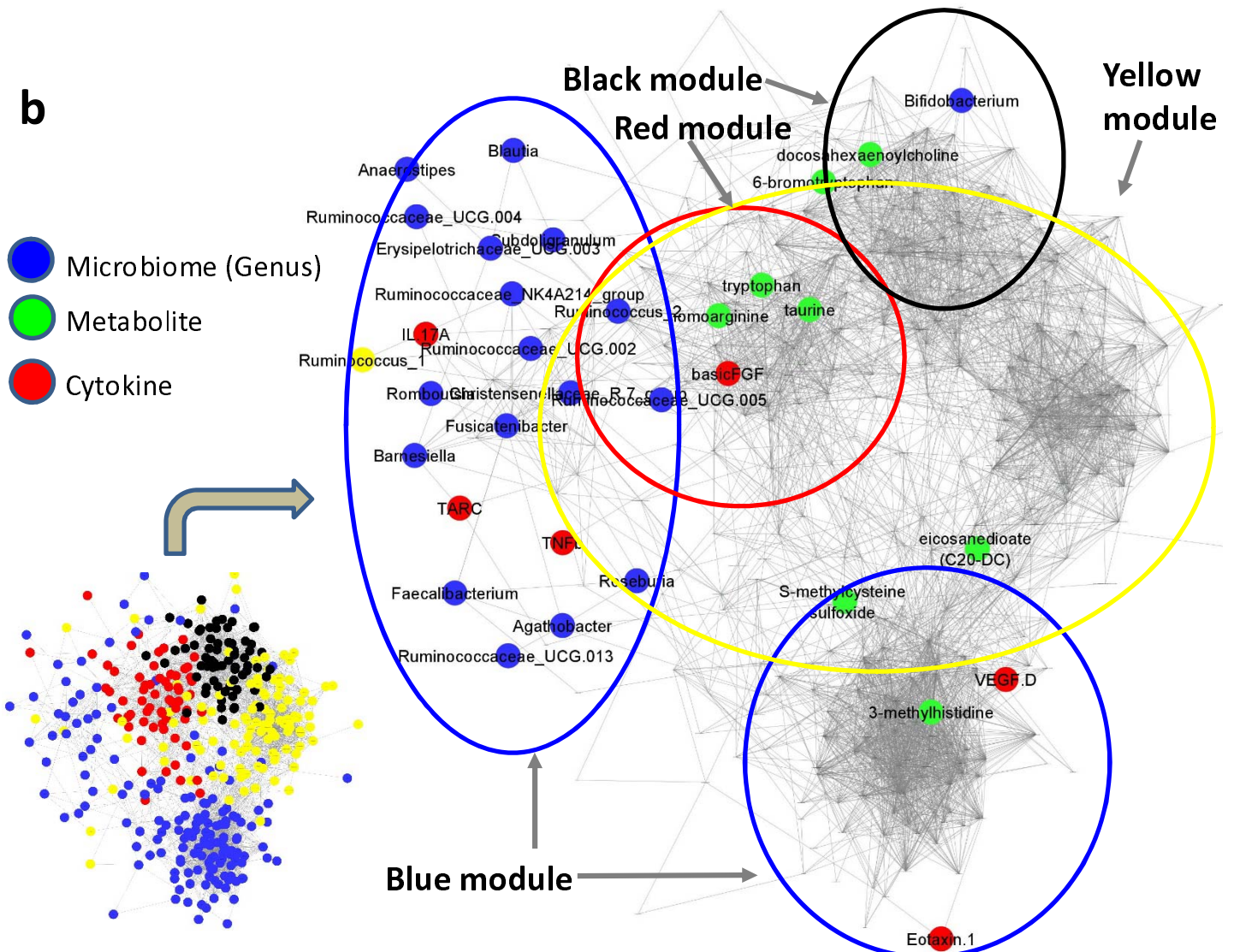
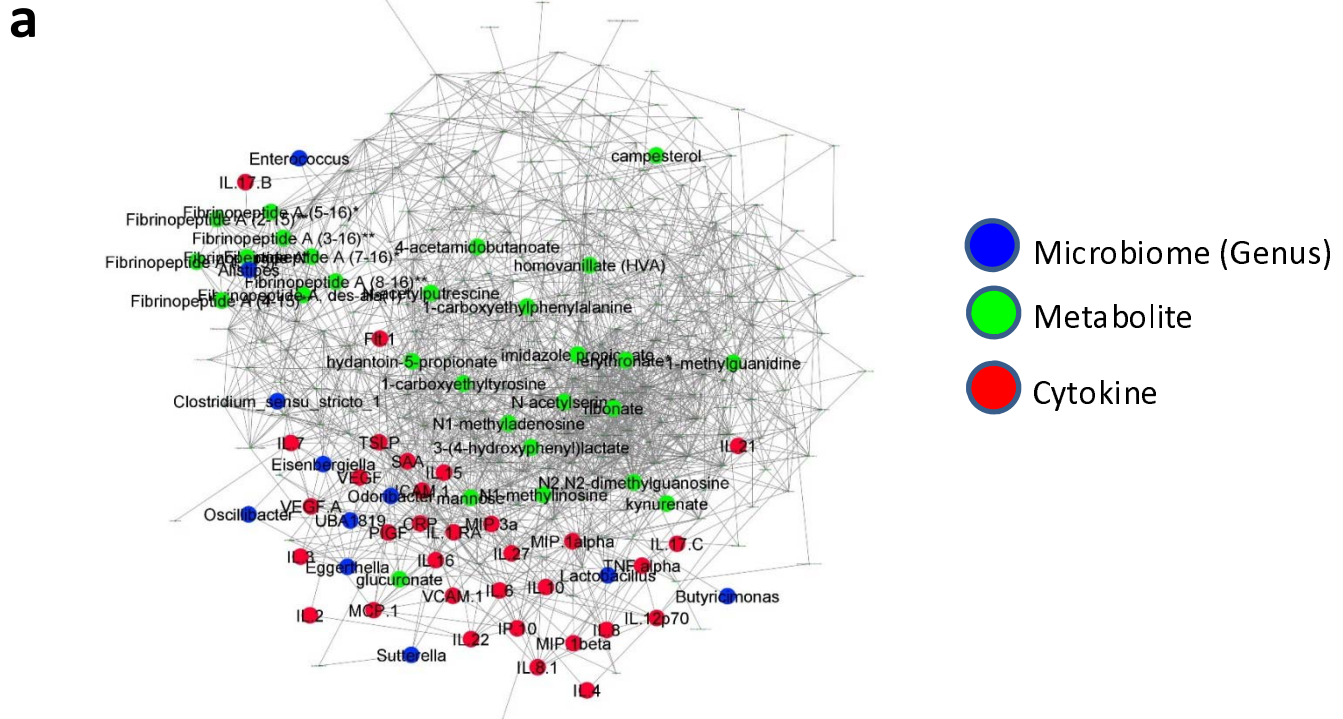
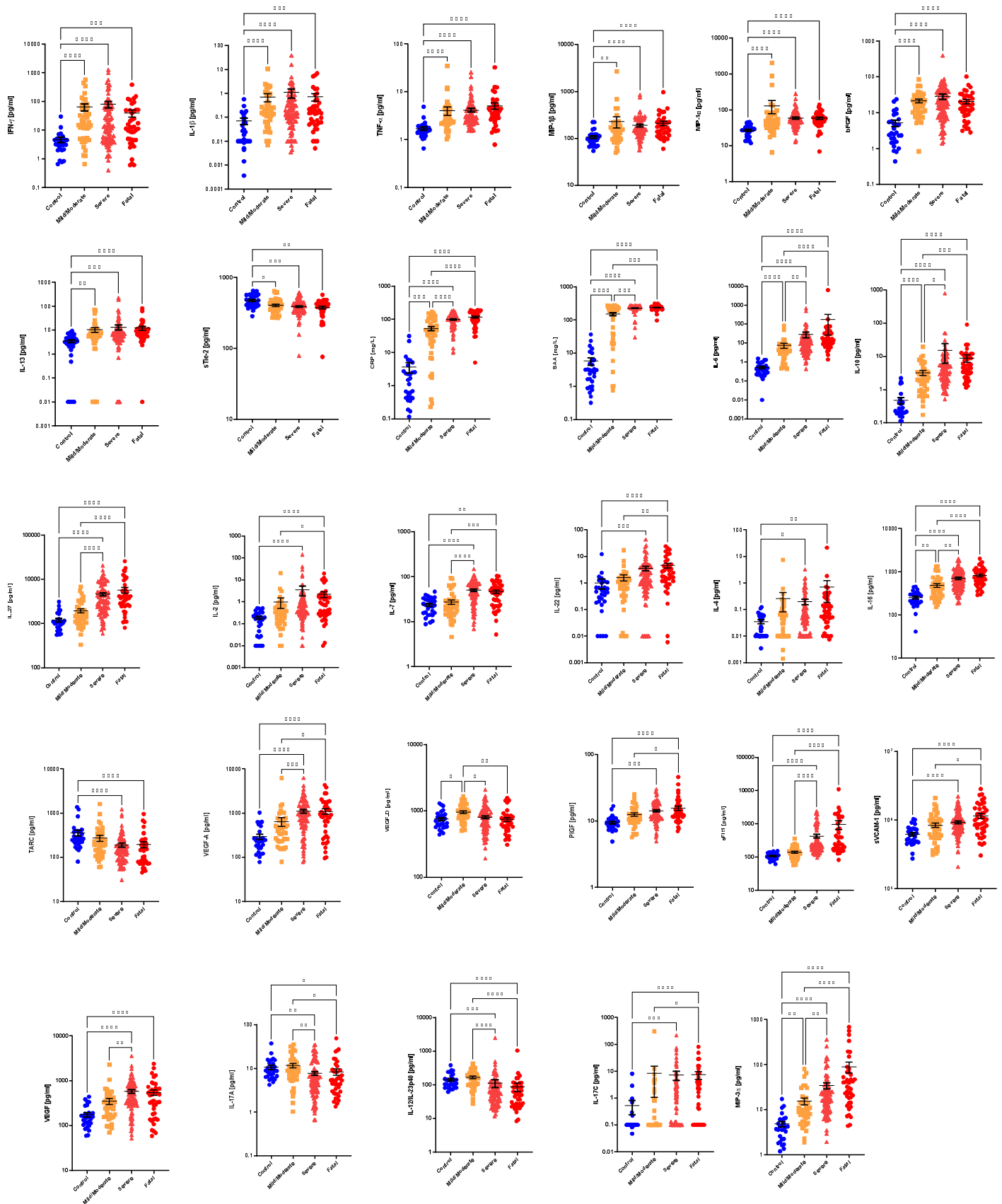


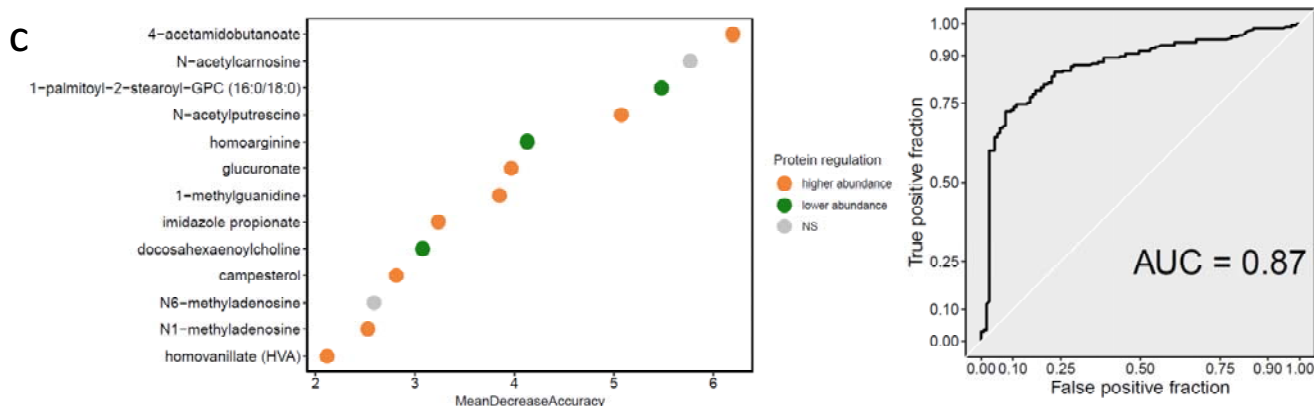
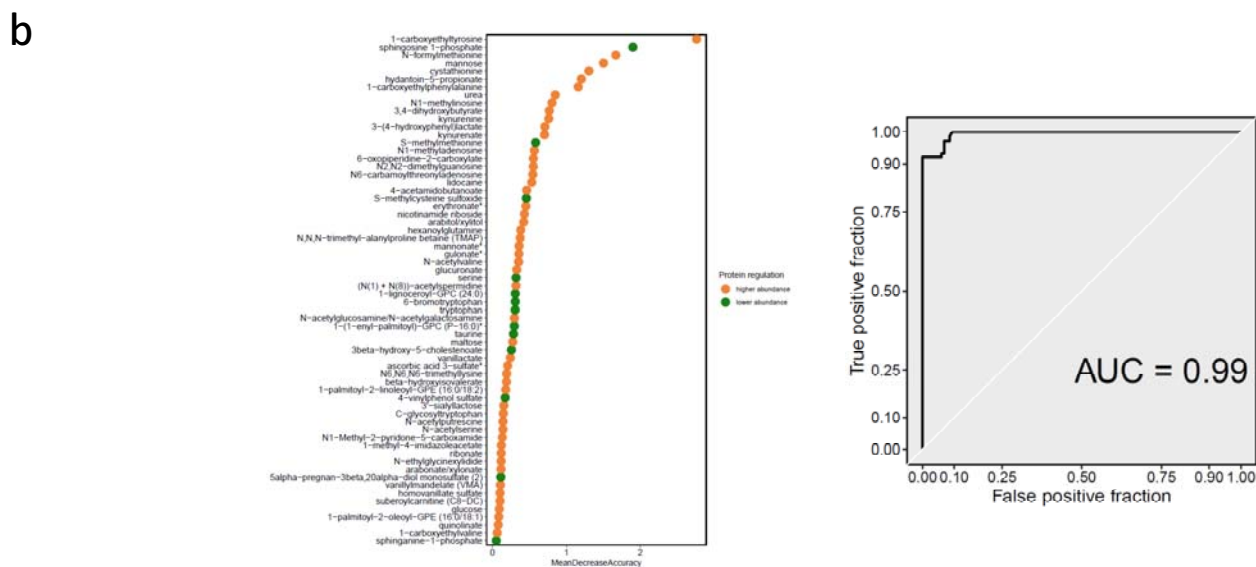
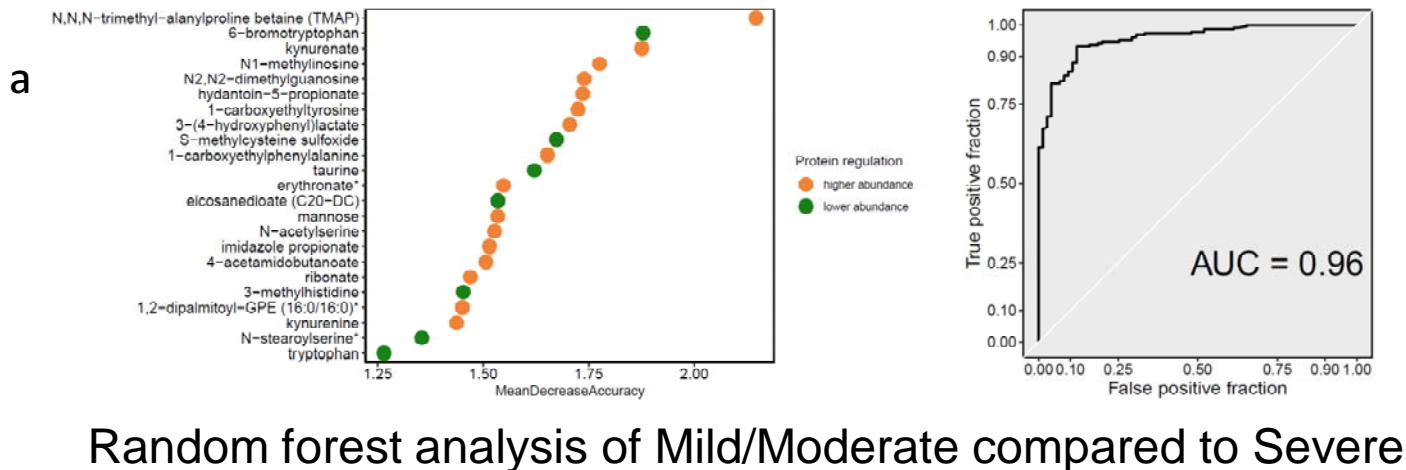
Fig. 5



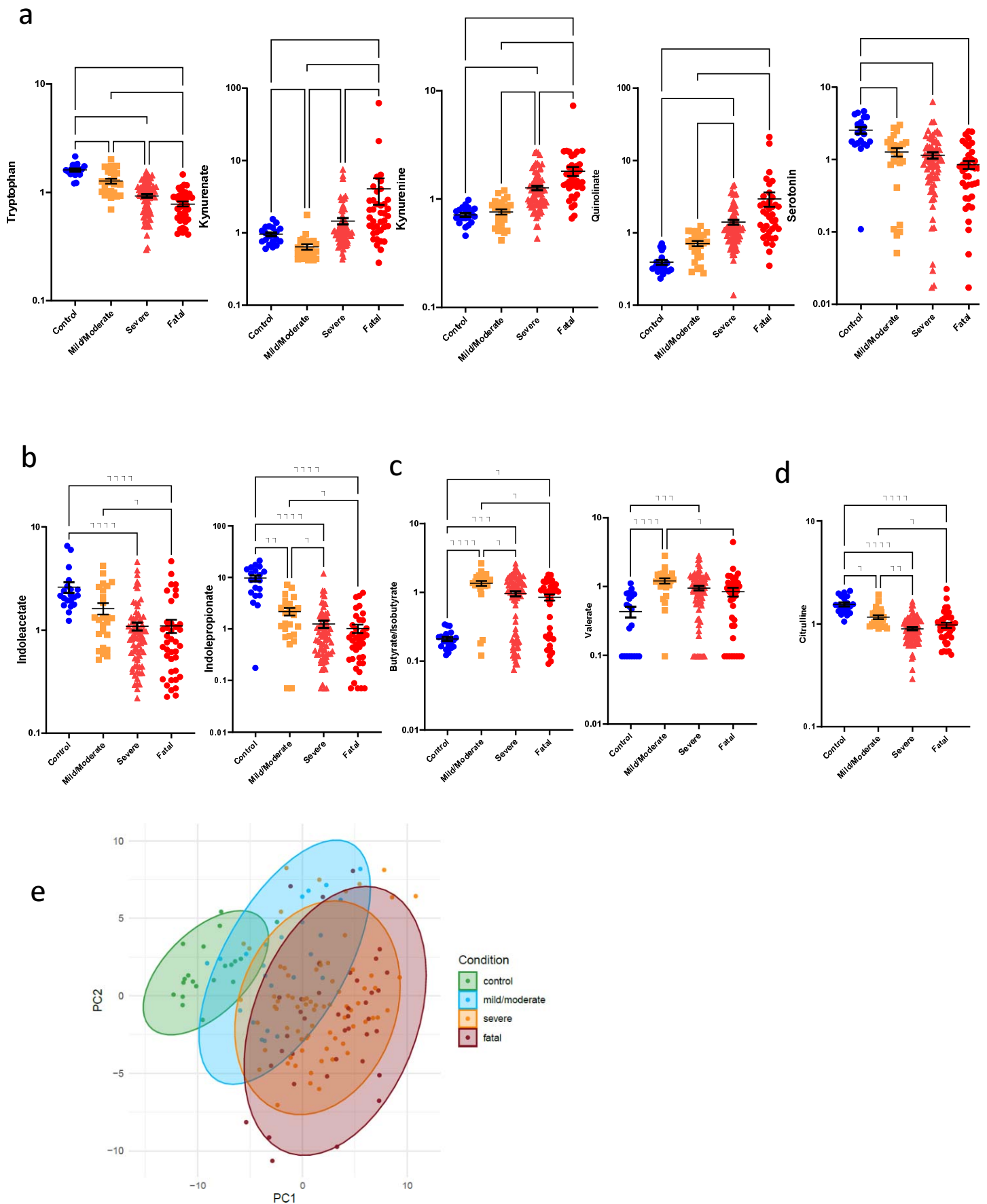
Supplementary Fig. 1



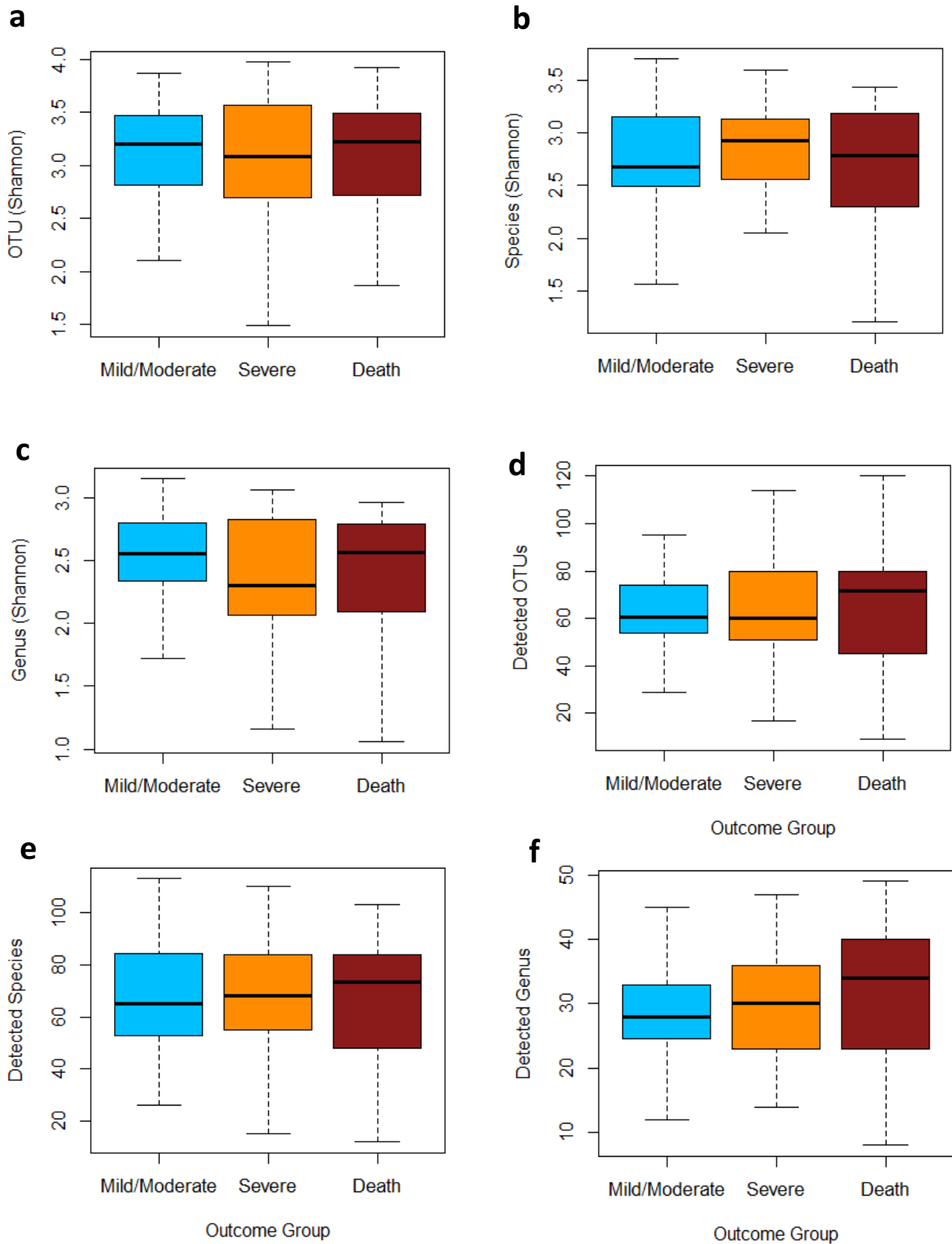
Supplementary Fig. 2



Supplementary Fig. 3

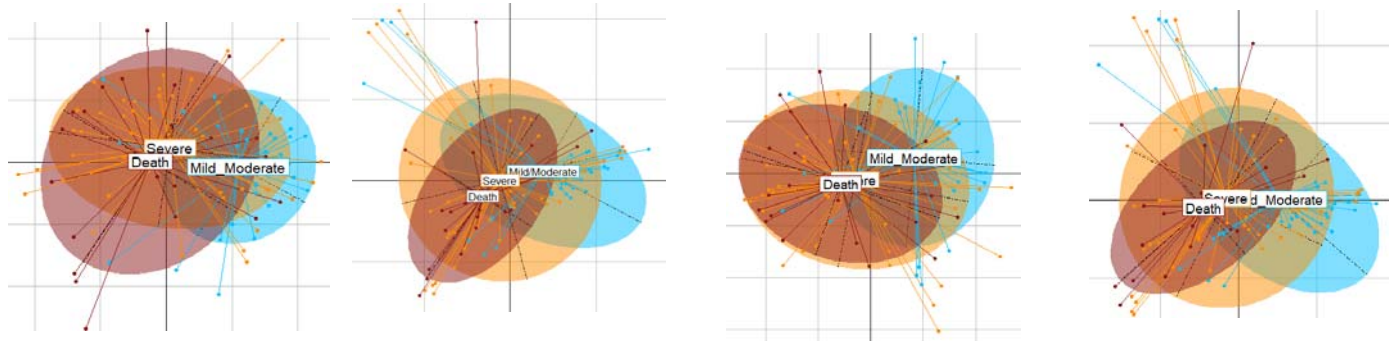


Supplementary Fig. 4



Supplementary Fig. 5

a OTU-Level



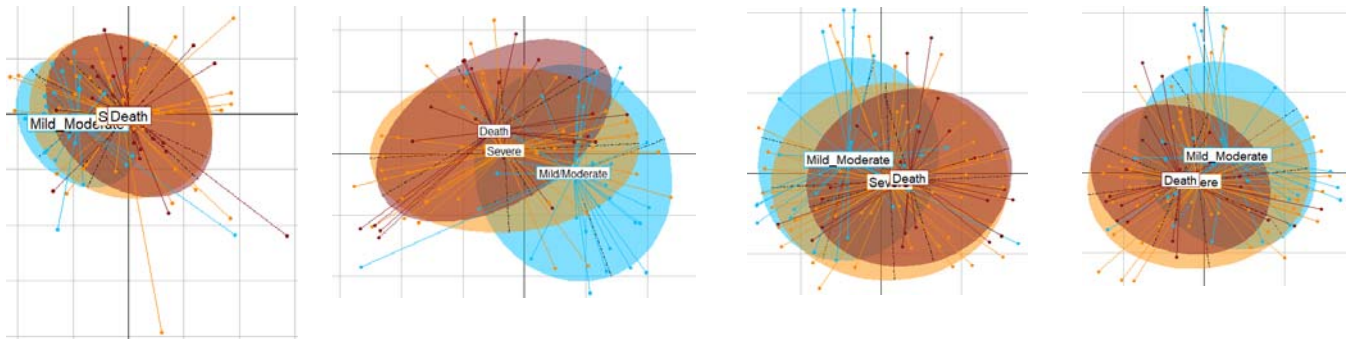
Spearman
Distance

Canberra
Distance

Bray-Curtis
Distance

Jaccard
Distance

b Species-level



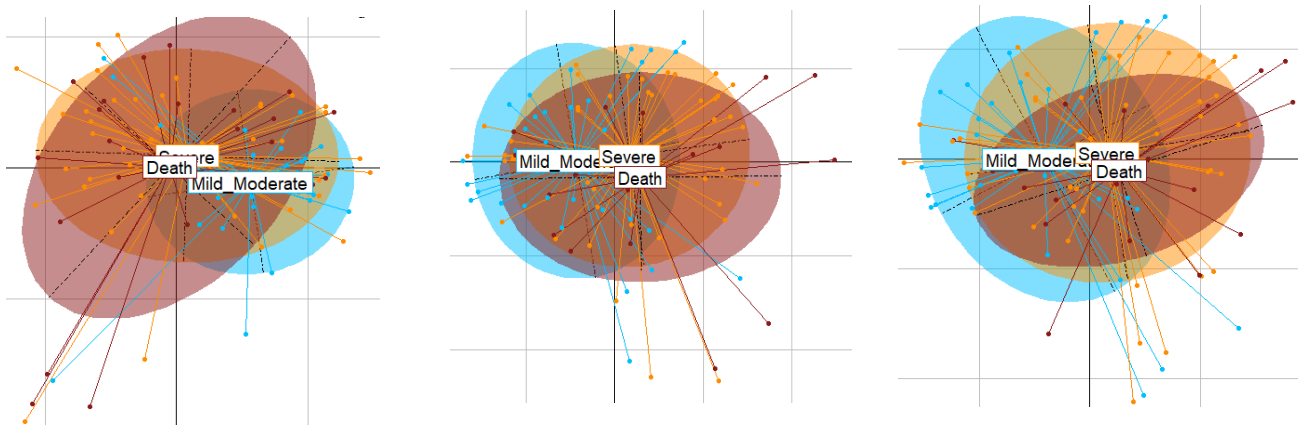
Spearman
Distance

Canberra
Distance

Bray-Curtis
Distance

Jaccard
Distance

c Genus-level

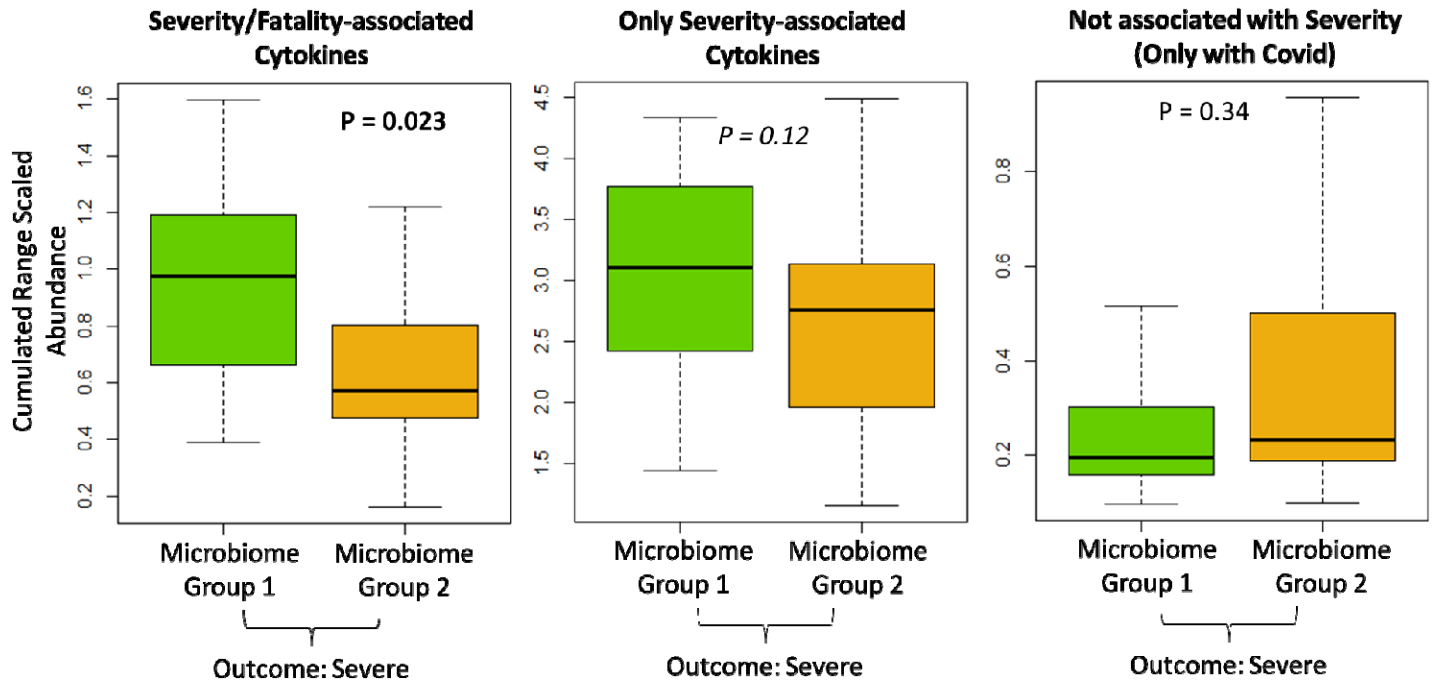


Spearman Distance

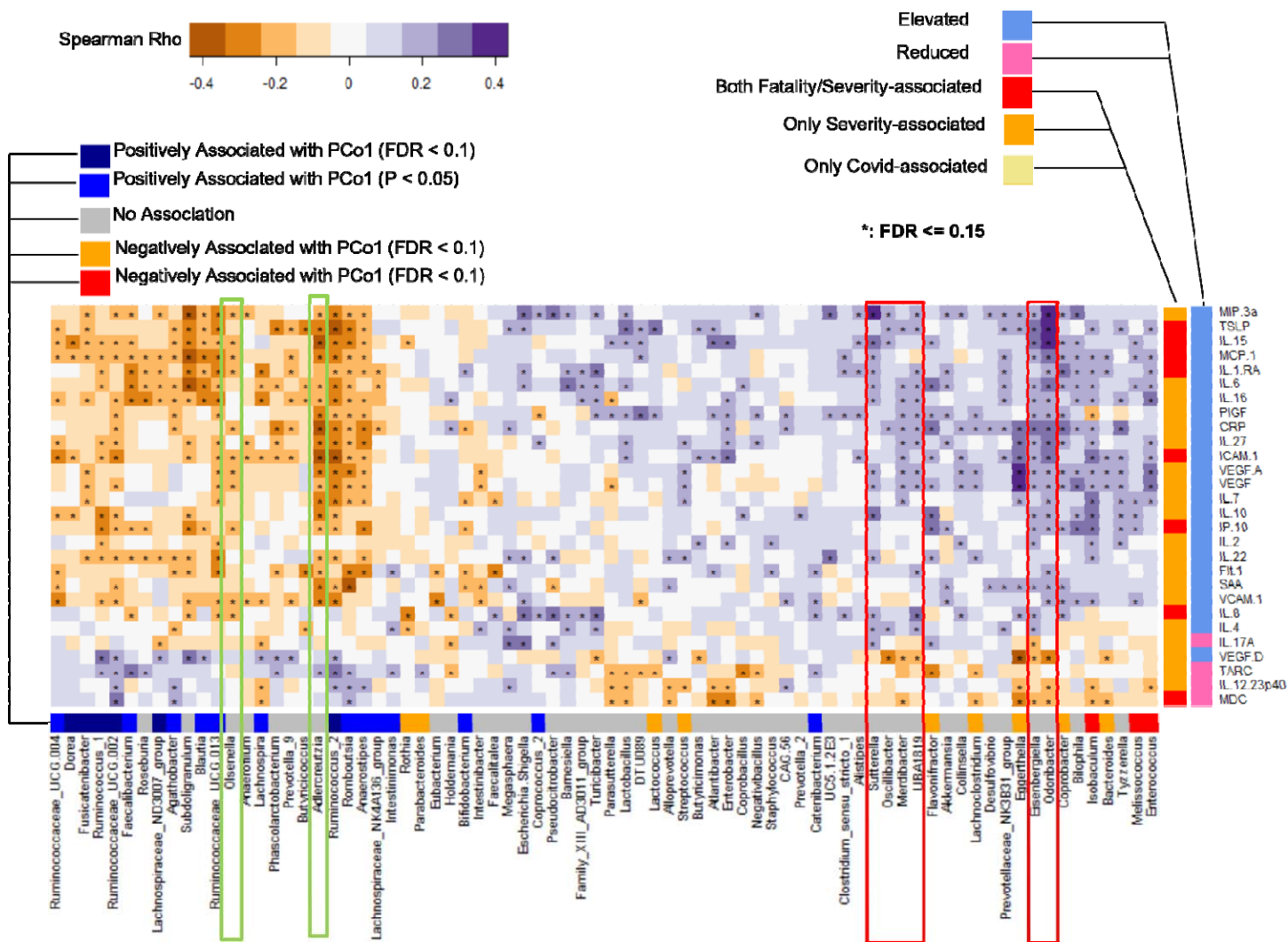
Bray-Curtis Distance

Jaccard Distance

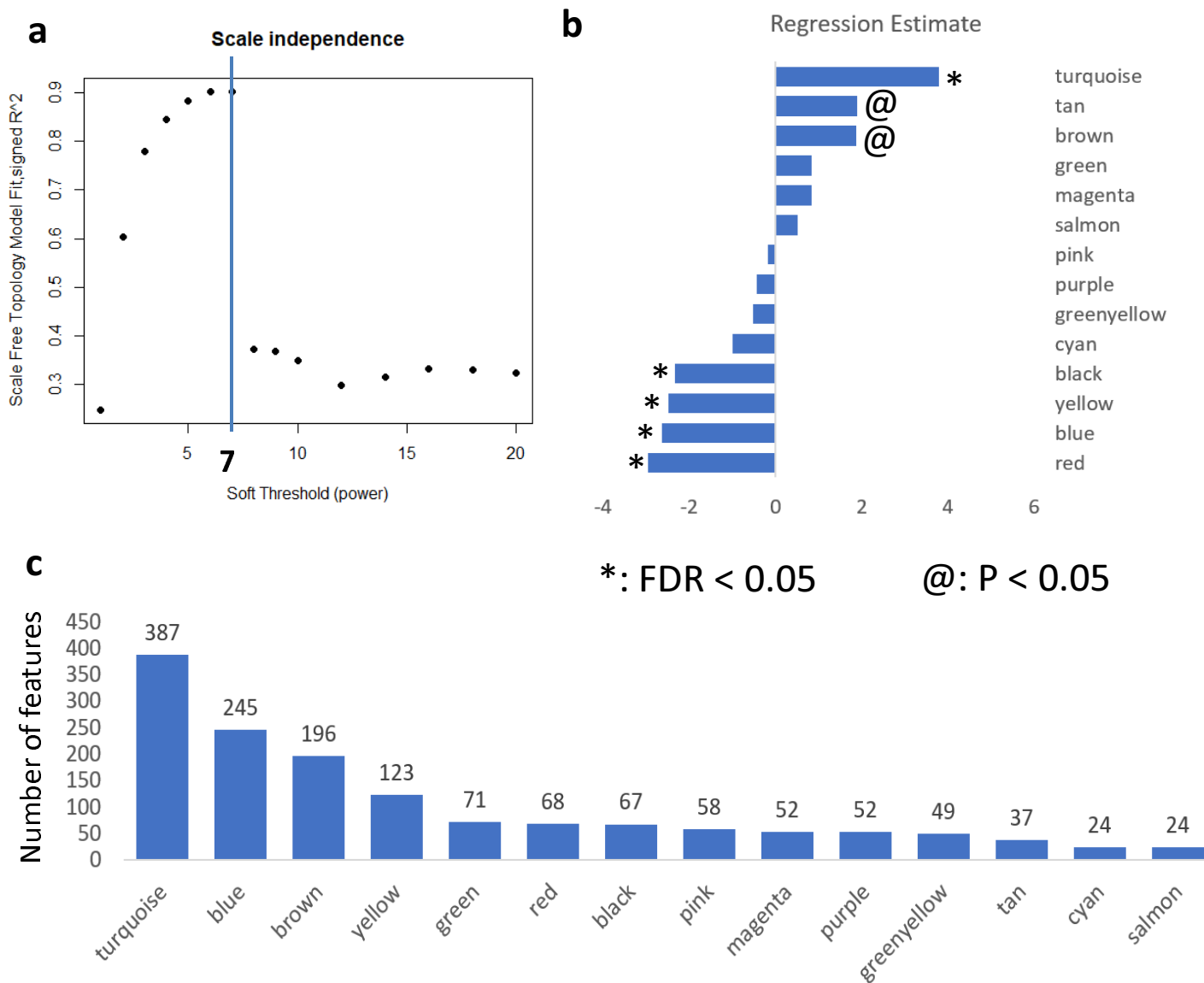
Supplementary Fig. 6



Supplementary Fig. 7

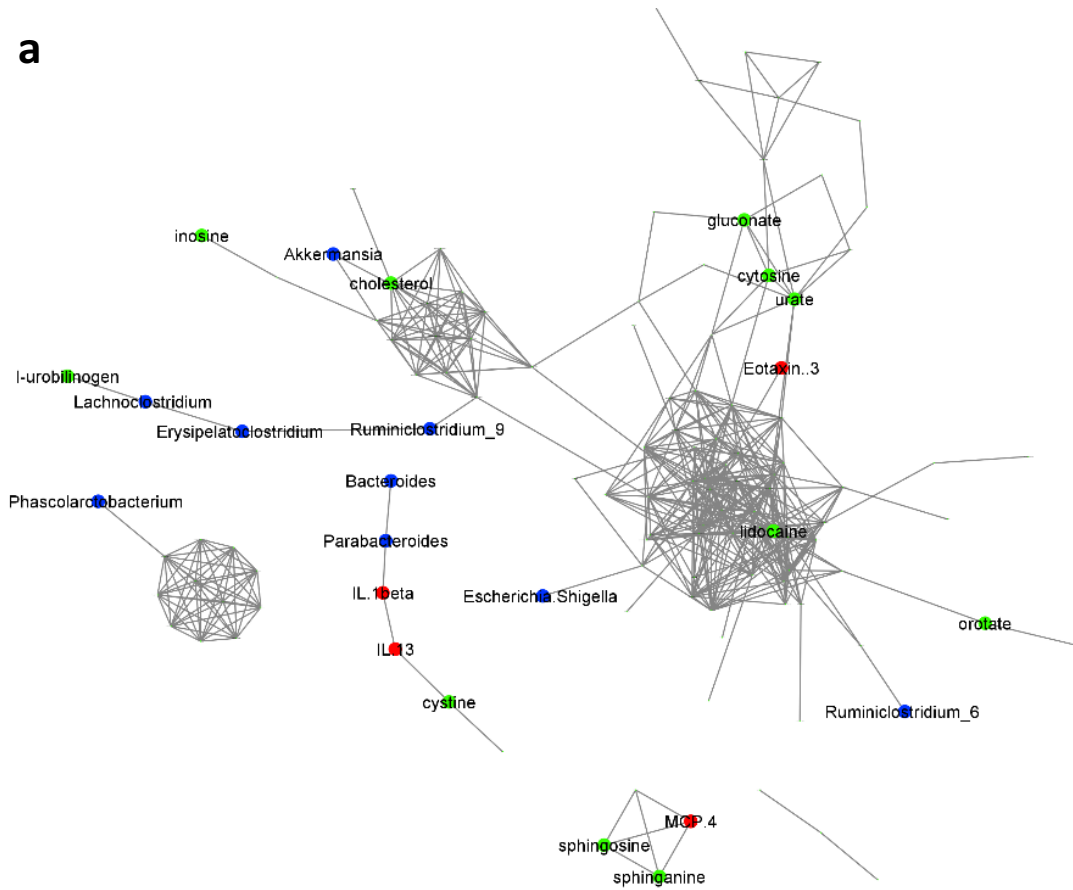


Supplementary Fig. 8

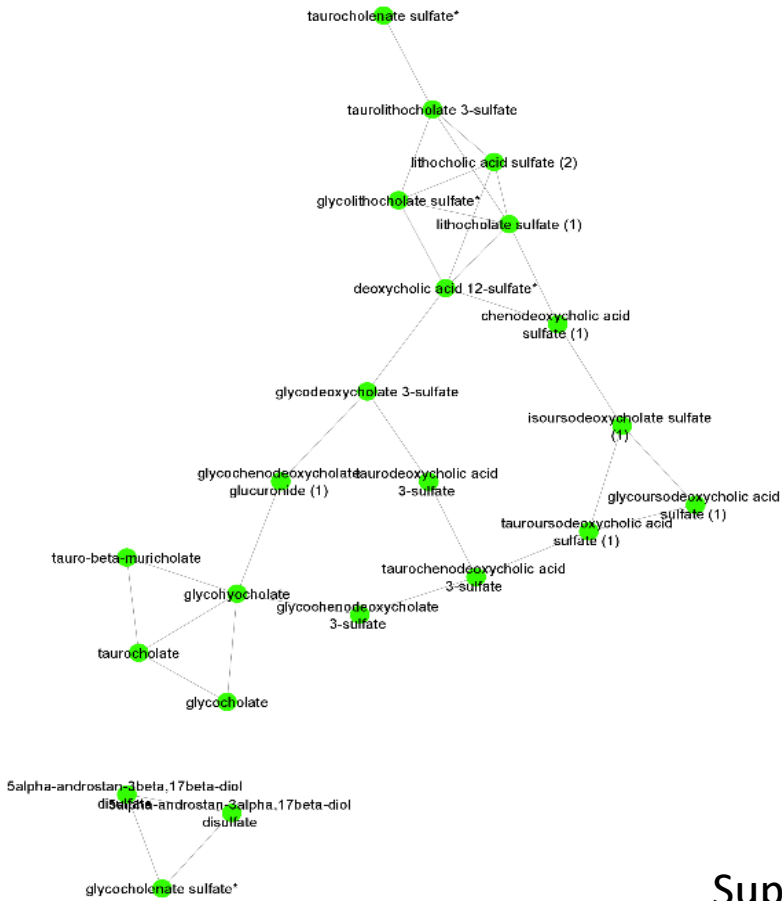


Supplementary Fig. 9

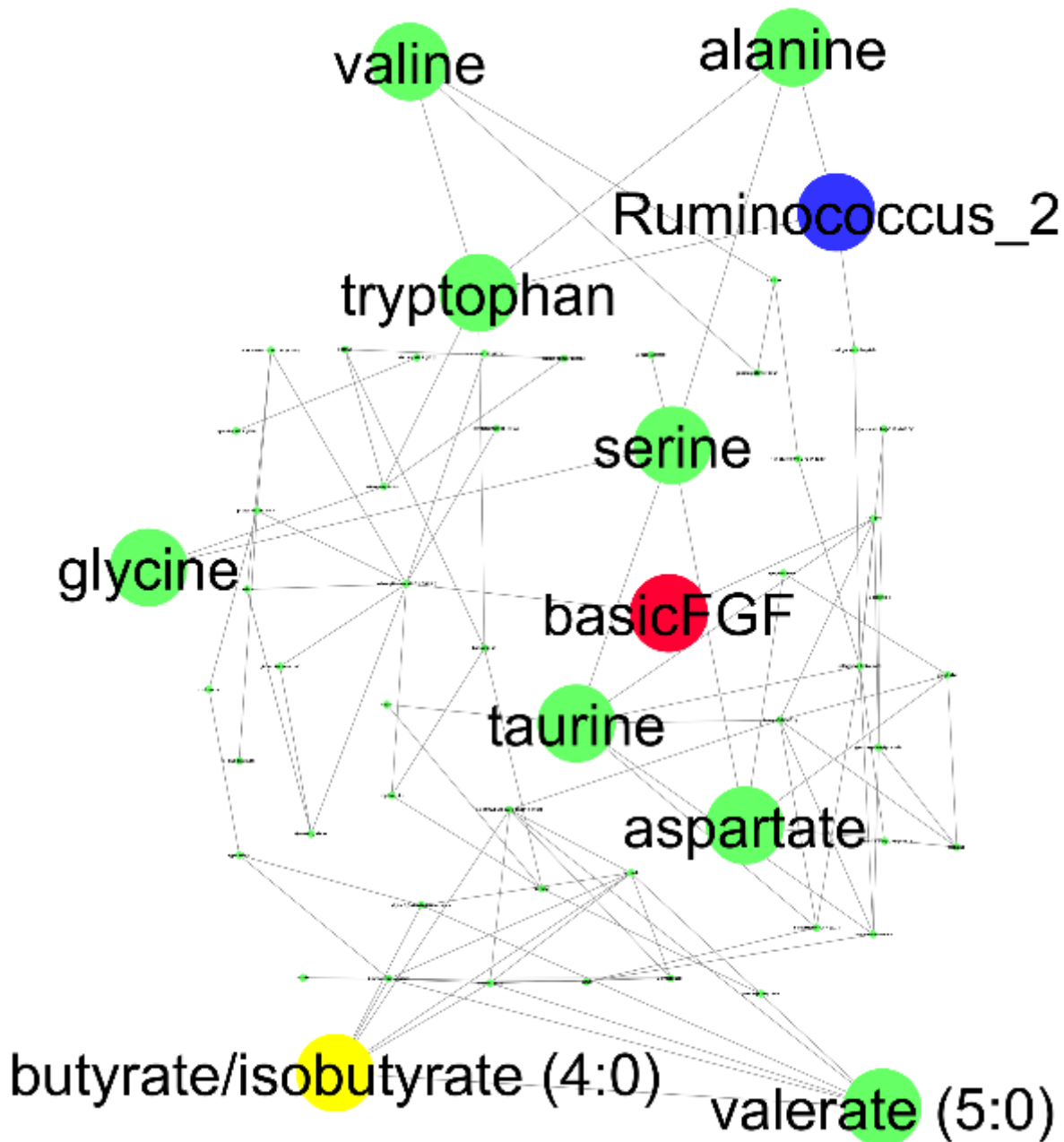
a



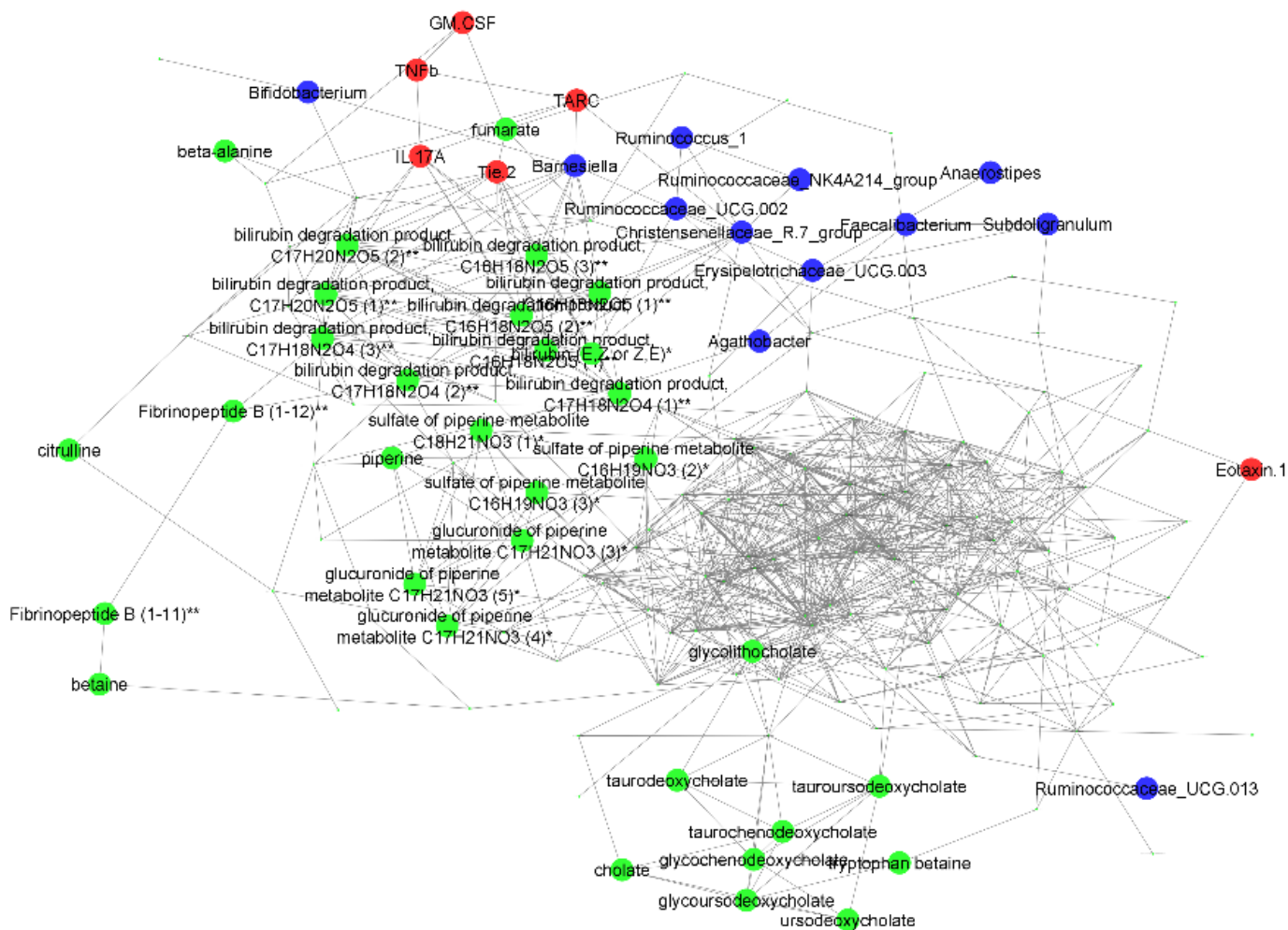
b



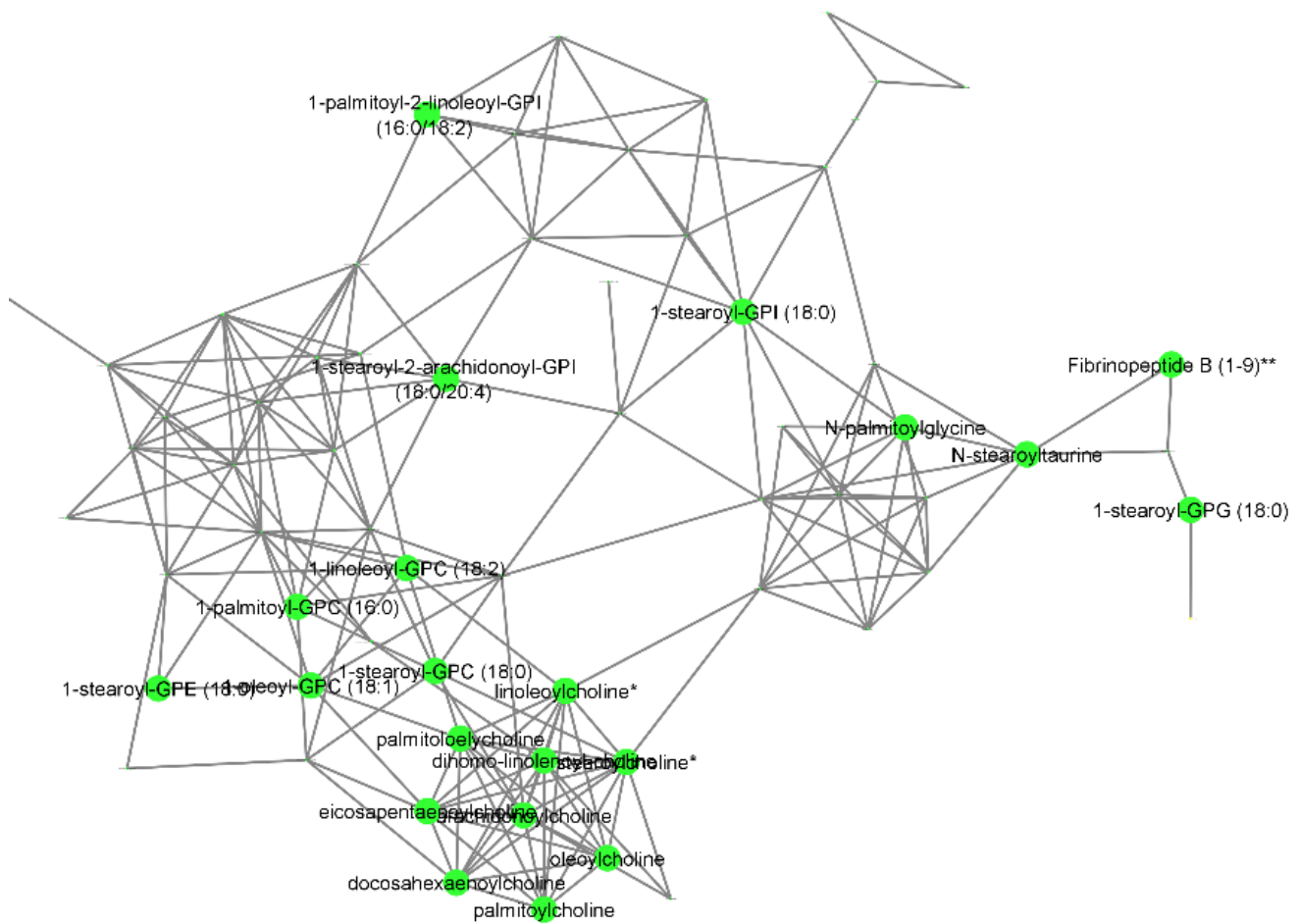
Supplementary Fig. 10



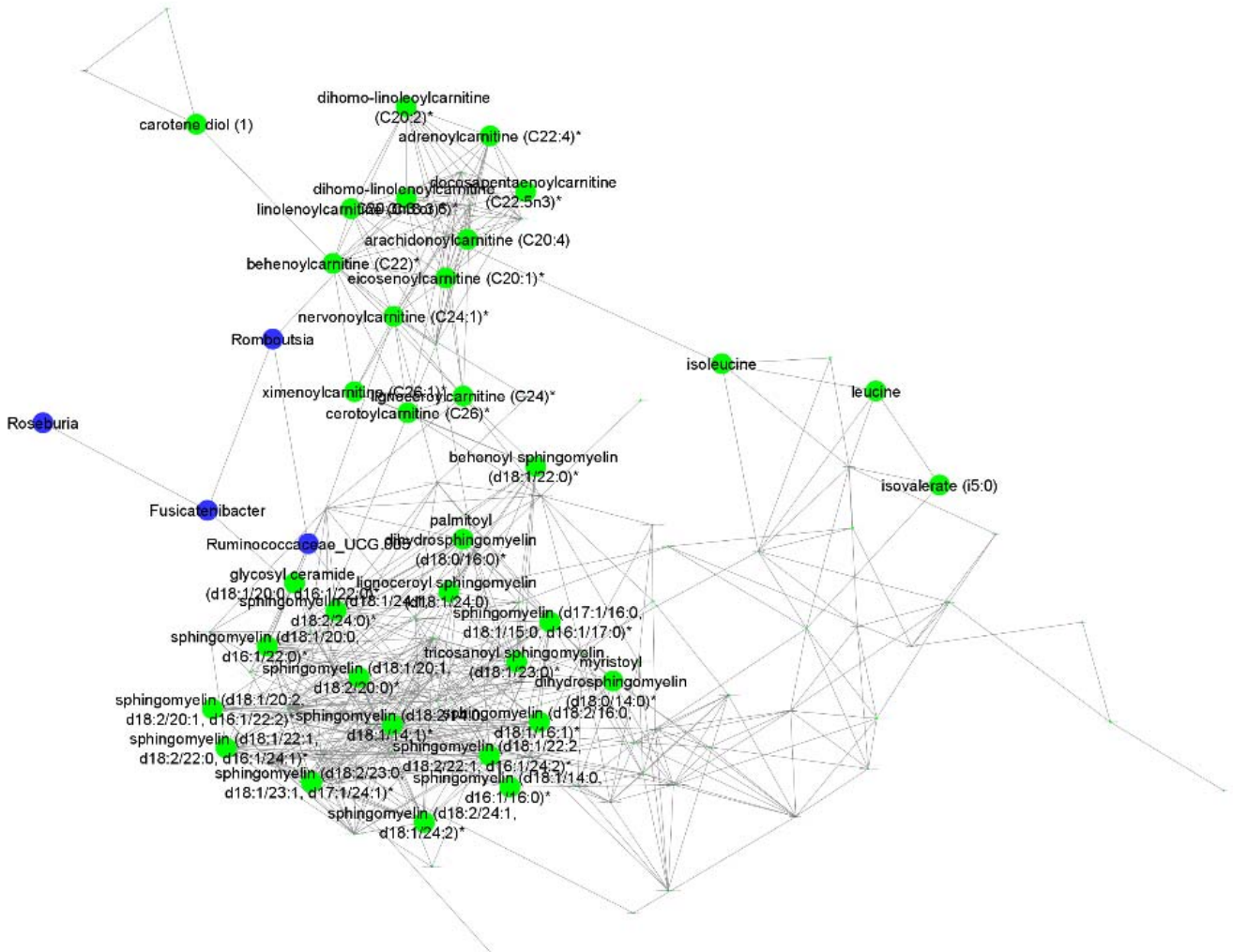
Supplementary Fig. 11



Supplementary Fig. 12



Supplementary Fig. 13



Supplementary Fig. 14